EXPERIMENTAL CHARACTERIZATIONS OF THE RESPONSE OF NEMATIC LIQUID CRYSTAL DROPLETS UPON ADSORPTION OF NANOPARTICLES FROM AQUEOUS MEDIA

A THESIS SUBMITTED TO
THE GRADUATE SCHOOL OF NATURAL AND APPLIED SCIENCES
OF
MIDDLE EAST TECHNICAL UNIVERSITY

BY

SELİN ŞENGÜL

IN PARTIAL FULFILLMENT OF THE REQUIREMENTS
FOR
THE DEGREE OF MASTER OF SCIENCE
IN
CHEMICAL ENGINEERING

SEPTEMBER 2021

Approval of the thesis:

EXPERIMENTAL CHARACTERIZATIONS OF THE RESPONSE OF NEMATIC LIQUID CRYSTAL DROPLETS UPON ADSORPTION OF NANOPARTICLES FROM AQUEOUS MEDIA

submitted by **SELİN ŞENGÜL** in partial fulfillment of the requirements for the degree of Master of Science in Chemical Engineering**, Middle East Technical University** by,

Prof. Dr. Halil Kalıpçılar
Dean, Graduate School of **Natural and Applied Sciences** _____

Prof. Dr. Pınar Çalık
Head of the Department, **Chemical Engineering** _____

Asst. Prof. Dr. Emre Büküşoğlu
Supervisor, **Chemical Engineering, METU** _____

Prof. Dr. Nihal Aydoğan
Co-Supervisor, **Chemical Engineering, Hacettepe University** _____

Examining Committee Members:

Assoc. Prof. Dr. İrem Erel Göktepe
Chemistry, METU _____

Asst. Prof. Dr. Emre Büküşoğlu
Chemical Engineering, METU _____

Prof. Dr. Nihal Aydoğan
Chemical Engineering, Hacettepe University _____

Assoc. Prof. Dr. Pınar Zeynep Çulfaz-Emecen
Chemical Engineering, METU _____

Assoc. Prof. Dr. Berna Topuz
Chemical Engineering, Ankara University _____

Date: 08.09.2021

I hereby declare that all information in this document has been obtained and presented in accordance with academic rules and ethical conduct. I also declare that, as required by these rules and conduct, I have fully cited and referenced all material and results that are not original to this work.

Name, Last name : Selin Şengül

Signature:

ABSTRACT

EXPERIMENTAL CHARACTERIZATIONS OF THE RESPONSE OF NEMATIC LIQUID CRYSTAL DROPLETS UPON ADSORPTION OF NANOPARTICLES FROM AQUEOUS MEDIA

Şengül, Selin
Master of Science, Chemical Engineering
Supervisor : Asst. Prof. Dr. Emre Büküşoğlu
Co-Supervisor: Prof. Dr. Nihal Aydoğan

September 2021, 61 pages

Nematic liquid crystal (LC) droplets have been widely used for the detection of molecular species. In this study, we investigated the response of micrometer sized nematic LC droplets against the adsorption of nanoparticles from aqueous media. In the first part of this study, we synthesized ~100 nm-in-diameter silica nanoparticles and modified their surfaces to mediate either planar or homeotropic LC anchoring and a pH-dependent charge. Secondly, we carried out the adsorption of nanoparticles to the LC-aqueous interface and investigated the response of LC droplets upon adsorption. We showed surface functionality- and concentration-dependent configurations of the droplets consistent with the change in the surface anchoring and the formation of local heterogeneities upon adsorption of the nanoparticles to LC-aqueous interfaces. According to our results, the adsorption of nanoparticles modified with dimethyloctadecyl [3-(trimethoxysilyl) propyl] ammonium chloride (DMOAP, homeotropic) exhibit a transition from bipolar to radial, whereas the adsorption of -COOH-terminated counterparts (planar) did not cause a configuration transition. By manipulating the electrostatic interactions, we controlled the

adsorption of the nanoparticles to the LC-aqueous interfaces, providing access to the physicochemical properties of the nanoparticles. We demonstrated a temporal change in the droplet configurations caused by the adsorption of the nanoparticles functionalized with -COOH/DMOAP mixed monolayers. These results provide a basis for studies in applications for the detection of nano-sized species, for sensing applications that combine nanoparticles with LCs, and for the synthesis of anisotropic composite particles with complex structures.

Keywords: Liquid crystals, nanoparticles, adsorption, response, emulsions

ÖZ

NEMATİK SIVI KRİSTAL DAMLACIKLARININ SULU ORTAMDAN NANOPARTİKÜL ADSORPSİYONUNA VERDİĞİ TEPKİLERİN DENEYSEL KARAKTERİZASYONU

Şengül, Selin
Yüksek Lisans, Kimya Mühendisliği
Tez Yöneticisi: Dr. Öğretim Üyesi Emre Büküşoğlu
Ortak Tez Yöneticisi: Prof. Dr. Nihal Aydoğan

Eylül 2021, 61 sayfa

Nematik sıvı kristal damlacıkları, moleküler türlerin tespiti için yaygın olarak kullanılmaktadır. Bu çalışmada, sulu ortamdan nanopartiküllerin adsorpsiyonuna karşı mikrometre boyutlu nematik sıvı kristal damlacıklarının tepkisini araştırdık. Bu çalışmanın ilk bölümünde, ~100 nm çapında silika nanoparçacıkları sentezledik ve yüzeylerini düzlemsel veya homeotropik sıvı kristal çapalanmasına ve pH'a bağlı bir yüke sahip olacak şekilde değiştirdik. İkinci olarak, nanopartiküllerin sıvı kristal-sulu arayüze adsorpsiyonunu gerçekleştirdik ve sıvı kristal damlacıklarının adsorpsiyon üzerine tepkisini araştırdık. Nanopartiküllerin sıvı kristal-su arayüzlerine adsorpsiyonu ile yüzey çapalanmasındaki değişiklik ve bölgesel heterojenitelerin oluşumu ile tutarlı olarak damlacıkların yüzey işlevselliğine ve konsantrasyona bağlı konfigürasyonlarını gösterdik. Sonuçlarımıza göre, -COOH ile fonksiyonlanmış nanopartiküllerin (düzlemsel) adsorpsiyonu damlacık konfigürasyonlarında bir değişime neden olmazken, dimetiloktadesil [3-(trimetoksisilil) propil] amonyum klorür (DMOAP, homeotropik) ile fonksiyonlanmış nanopartiküllerin adsorpsiyonu ile damlacık konfigürasyonlarındabipolardan radyale geçiş görüldü. Elektrostatik etkileşimleri

manipüle ederek, nanopartiküllerin fizikokimyasal özelliklerine erişim sağladık ve nanopartiküllerin sıvı kristal-su arayüzlerine adsorpsiyonunu kontrol ettik,. Damlacık konfigürasyonlarında -COOH/DMOAP karışık tektabakaları ile işlevselleştirilmiş nanoparçacıkların adsorpsiyonunun neden olduğu geçici bir değişiklik olduğunu gösterdik. Bu sonuçlar, nano boyutlu türlerin tespiti, nanoparçacıkları sıvı kristaller ile birleştiren tespit uygulamaları ve karmaşık yapılara sahip anizotropik kompozit parçacıkların sentezi için yapılan çalışmalara bir temel sağlamaktadır.

Anahtar Kelimeler: Sıvı kristaller, nanopartiküller, adsorpsiyon, tepki, emülsiyonlar

To my family

ACKNOWLEDGEMENTS

Firstly, I would like to express my deepest gratitude to my advisor Dr. Emre Bukusoglu for his support, guidance and patience throughout this study. I would also like to express my sincere gratitude to my co-supervisor Prof. Dr. Nihal Aydogan for her support and helpful suggestions.

I would also like to thank to Soft and Functional Materials Laboratory Group members; Aslı Karausta, Özge Batır, Burak Akdeniz, Deniz Avşar, Ceren Kocaman, Elif Kurt, Umut Dinç, Elif Erçelik, Ali Akman and Pınar Beyazkılıç Ayas for all the support and patience that they show during my study. I am fortunate to have been a part of this group and have labmates that makes me feel like we are a family.

Also, I would like to thank my dear friends İrem Tuğçe Korkut, Emre İlik, Toprak Çağlar, Mehmet Can Oflaz, Ayşe Akdeniz, Süleyman Goksu, Kübra Sarp, Mehmet Çoban, Hüseyin Macit, Sedef Özen and Selin Durmuş for their friendship and endless support during my graduate study.

Most importantly, my family deserves endless gratitude for their support that keeps me motivated and confident from the beginning until the end. Deepest thanks to Saliha, Semih, Sercan and Esra Şengül for always being there for me. I simply couldn't have done this without you.

Lastly, special thanks to Mert Fırtın for the unconditional love, encouragement and patience during this study and every day.

For financial supports, I would like to thank the Scientific and Technological Research Council of Turkey (TÜBİTAK) under the award number 219M068.

TABLE OF CONTENTS

LIST OF FIGURES

FIGURES

CHAPTER 1

INTRODUCTION

Liquid crystal (LC) based sensors have received remarkable attention due to their label-free, energy-free and sensitive applications. To date, LC-based sensors have been developed using both solid and aqueous interfaces. Although both systems have different attributes that can be used in sensing applications, LC-aqueous interface is preferable due toits favorable characteristics such as high mobilty of molecules at the surface and its high deformability.

Liquid crystal is a state of matter between crystalline solid and an isotropic liquid. They exhibit fluidic properties of isotropic liquids and long range orientational ordering of crystalline solids. LCs defined as thermotropic when their phase transitions are determined by temperature.[1] The mobility of thermotropic LCs increases with temperature. Thus, they lose their orientational order and their phase changes to isotropic. In nematic phases of thermotropic LCs, molecules align in a uniform direction called director without any positional order.

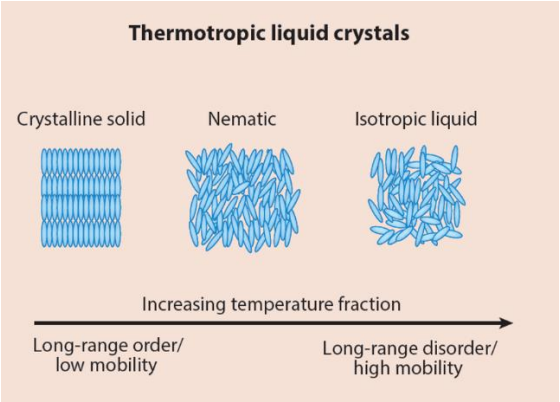

Figure 1.1 Schematic illustration of the phase behaviour of thermotropic LCs depending on temperature. Reprinted with permission from Reference 1. Copyright 2016 Annual Reviews.

The orientation of LC molecules changes depending on the three key concepts that defines liquid crystal behavior which are surface anchoring, elasticity and topological defects. The surface anchoring is related to the intermolecular interactions between LC mesogens and the confining medium. In the absence of an external field, LC molecules align in the easy axis which is the lowest free energy orientation of the LC director. The application of an external field causes deviation of the director from the easy axis and leads to an increase in the free energy of the interface. Interfacial free energy simply described as;

$$F_s = F_0 + \frac{1}{2} W_a sin^2(\theta_s - \theta_e) \qquad \text{(Equation 1)}$$

Where W_a is the surface anchoring energy, θ_s and θ_e are the angles defining the orientations of the director and easy axis, respectively. Owing to this concept, LC alignment can be tuned by functionalization of surfaces contacting with LC. Two types of surface anchoring formed depending on the alignment of LC molecules to the interface. In homeotropic anchoring, LC molecules align perpendicularly to the interface. On the contrary, planar anchoring formed when the alignment is parallel to the surface.

Second key concept is the elasticity of LCs which provides long-range orientational ordering to LCs. There are three main strain modes of LCs which are splay, twist and bend. The elastic-free energy density described using Frank-Oseen equation:

$$F_d = \frac{1}{2} K_1 (\nabla \cdot n)^2 + \frac{1}{2} K_2 (n \cdot \nabla \times n)^2 + \frac{1}{2} K_3 (n \times (\nabla \times n))^2 \qquad \text{(Equation 2)}$$

Where K_1, K_2, and K_3 are the strain constants for splay, twist and bend states respectively.

Topological defects are discontinuity regions in LCs that form due to the confinement of LC within certain geometries. Within these geometries, LC molecules cannot satisfy the boundary conditions by the continuous strain of the LC and topological defects form. Schematic illustrations of different types of topological defects are given in Figure 1.2.

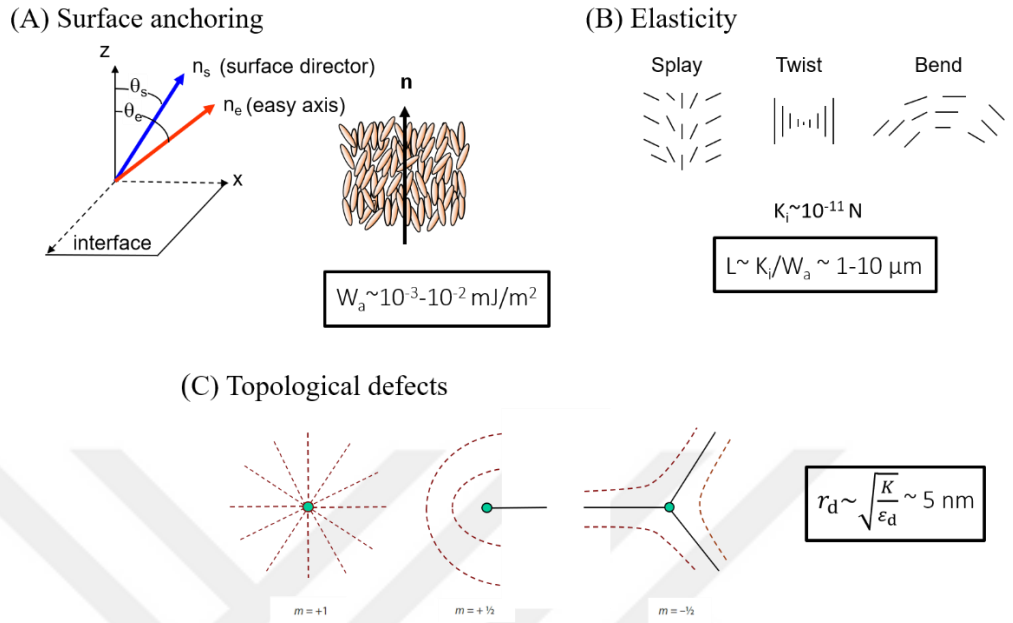

Figure 1.2 Key concepts of LCs. Schematic illustrations of (A) the director and easy axis of a LC anchored at a surface, (b) the three basic modes of deformation of a LC and (C) three types of topological defects that can form in a LC: (left) a point defect located at the center of a radially converging director field, and (center, right) cross-sections of line defects (disclinations). Reprinted with permission from Reference 1. Copyright 2016 Annual Reviews.

The balance between the key concepts of LC determines the director configuration of LCs. Confinement of LC within a spherical geometry leads to a competition between elastic and surface anchoring energies which causes the formation of topological defects. Due to the presence of defects that provide high sensitivity, LC emulsions are favorable among other geometries as they offer high responsiveness.[1,2] Various configurations can be obtained in LC droplets including bipolar, axial, escaped radial, preradial and radial resulting from this competition.[3,4] When dispersed in pure water, LC droplets exhibit bipolar configuration resulting from the planar anchoring of 5CB at the interface, which is characterized by two boojum defects located at the opposite poles of the droplets. Configuration change in LC droplets arises from the change in the anchoring of the LC at the LC-aqueous interface. When homeotropic anchoring induced on LC droplets, they exhibit radial

configuration. The radial configuration was identified with a point defect located at the center of the droplet and a four-petal appearance under polarized optical microscope. For the droplets maintaining anchoring conditions between planar and homeotropic, various equilibrium states obtained during the configuration transition of LC droplets from bipolar to radial. Firstly, two defects observed in bipolar configuration dissapeared and leads to the formation of axial configuration which is characterized by the line disclination appeared on the droplet surface. Then, due to the increase in the anchoring strength, disclination line present on the surface turns into a point defect and located at the the vicinity of the LC-water interface. This configurtion called as preradial and identified by an angle-dependent bright appearance of the droplets under polarized microscope. Lastly, before LC droplets adopting radial configuration which is an indicator of strong homeotropic anchoring in LCs, point defect located in a place between the center and surface of the droplet which is called escaped radial configuration.[5]

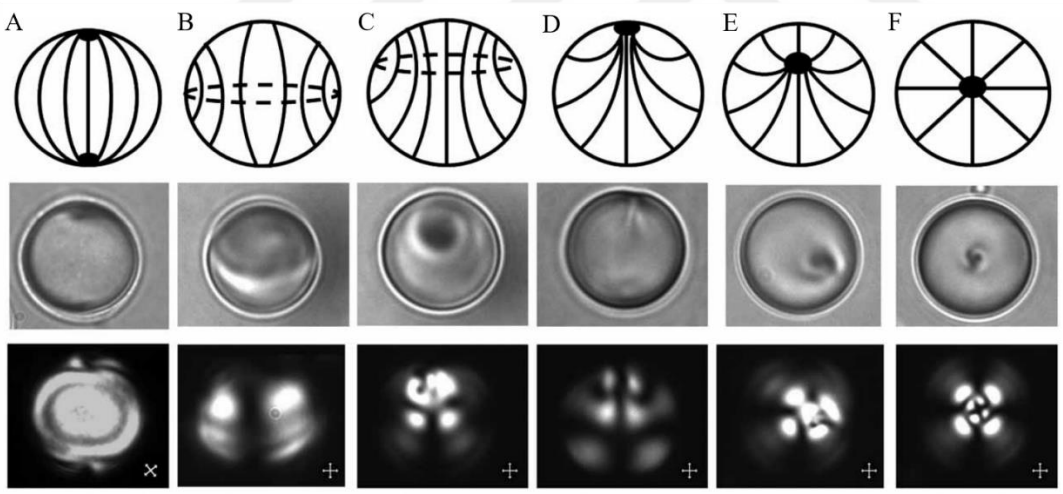

Figure 1.3 Schematic illustrations (top row), bright field (middle row) and polarized light (bottom row) micrographs of LC droplets maintaining (A) bipolar, (B, C) axial, (D) preradial (E) escaped radial and (F) radial configurations. Reprinted (adapted) with permission from Reference 5. Copyright 2009 American Chemical Society

Theoretically, the ratio of the elastic energy, which scales with ~KL (where K is the elastic constant with one constant approximation and L is the characteristic length scale), to surface anchoring energy, which scales with ~WL^2 (where W is the surface

anchoring energy) gives a characteristic size scale between 1 and 10 μm. In this range, competition between elastic energy and surface anchoring energy provide an optimum size range for LC droplets. Below this range, LC droplets adopt a strain-free, uniform director configuration while larger droplets maintain configurations which satisfies the surface anchoring conditions at their interfaces.[6] Even though their observations are not consistent with the theoretical predictions, size-dependent ordering transitions of LC droplets took part in experimental studies. In contrast to predictions, experimental observations reported the bipolar to radial ordering transition in LC droplets with decreasing droplet size.[7]

Many of the past studies examined the use of LC-aqueous interface to detect molecular species of proteins[8–10], lipids[11,12], surfactants[5,13–16], bacteria[17] and virus[17] present in aqueous media. In addition, interaction of LCs with microparticles and the organization of micrometer sized particles at LC-water interface have been studied.[18] As we mentioned above, considering the interplay of the elastic energy and surface anchoring energy the size scale close to 1 μm is critically important. This balance affects the behavior of particles when they introduced in LC medium. For the particles smaller than 1 μm, elastic energy dominates, and particles do not cause a change in the orientation of LC near them. In contrast, large particles distort the LC orientation in their vicinity to satisfy the anchoring conditions at their surfaces since surface anchoring energy dominates the system.[19] For the particles close to 1 μm, elastic and surface energy are competing. Therefore, nanoparticles interactions at the interfaces of LCs may differ from micro-sized particles and must be investigated.

Nanoparticles have gained considerable interest due to their unique properties.[20] They can be synthesized from a wide range of materials with different size, shape and surface properties. The high surface to volume ratio of nanoparticles enables effective functionalization of their surfaces. Functionalization of their surface improves the characteristic of nanoparticles allowing them to be used in various applications such as drug delivery[21], chemical and biological sensors[22], biomedical applications[23]. Beyond their technological importance, nanoscopic species that cover the size range of 10-100 nm are of particular interest as they cover the size scale that

are ubiquitous in microorganisms such as virus and bacteria. Viruses have various surface properties and charge distributions. Since nanoparticles show similarity with many species in nature regarding their sizes and surface properties, studies involving the detection of surface-modified nanoparticles may provide information for sensing applications of viruses showing similar characteristics.

In this study, we aim to carry out the adsorption of nanoparticles on LC droplets and investigate the configurations of LC droplets maintained upon adsorption. We are motivated to control the adsorption of nanoparticles on the interfaces of the nematic droplets and examine their configurations experimentally. Since nano-sized species have unique surface characteristics, we investigated surface-property dependent response of LC droplets to highlight the importance of our system in sensing applications. For this purpose, we used silica nanoparticles since their surfaces can easily be modified with different functional groups. Also, simple, scalable and low-cost production of silica nanoparticles makes their application favorable. We modified the surface of silica nanoparticles using silane groups that provide different characteristics to silica, such as hydrophobicity, hydrophilicity, surface anchoring and pH-dependent surface charge. Then, we carried out controlled adsorption of surface-modified nanoparticles. Lastly, we examined the adsorption of nanoparticles and investigated LC droplet response by optical and surface characterizations.

CHAPTER 2

LITERATURE REVIEW

LC-based materials are promising systems for sensing applications due to their responsive and dynamic nature. They possess various advantages over other technologies as they do not require complex instrumentation or chemical labeling techniques for the detection of molecules. LCs have used to detect a wide range of molecules as virus, bacteria and surfactants to date. LC-based sensors involve either the detection of targeted molecules presented on solid surfaces or the adsorption of molecules to LC/aqueous interfaces.[24]

Previous studies have reported the detection of molecules using LC-solid interfaces. Schwartz et al. used LCs to detect DNA molecules at solid surfaces.[25] They investigated the LC alignment change due to their interaction with DNA molecules presented on a solid surface. This study examined the interaction of single-stranded(ssDNA) and double-stranded(dsDNA) DNA with LCs. When LCs contacting with ssDNA, LC molecules align in the extension direction of ssDNA molecules. In contrast to ssDNA, dsDNA induces a change in the LC alignment at a tilted angle upon their interaction as shown in Figure 2.1.

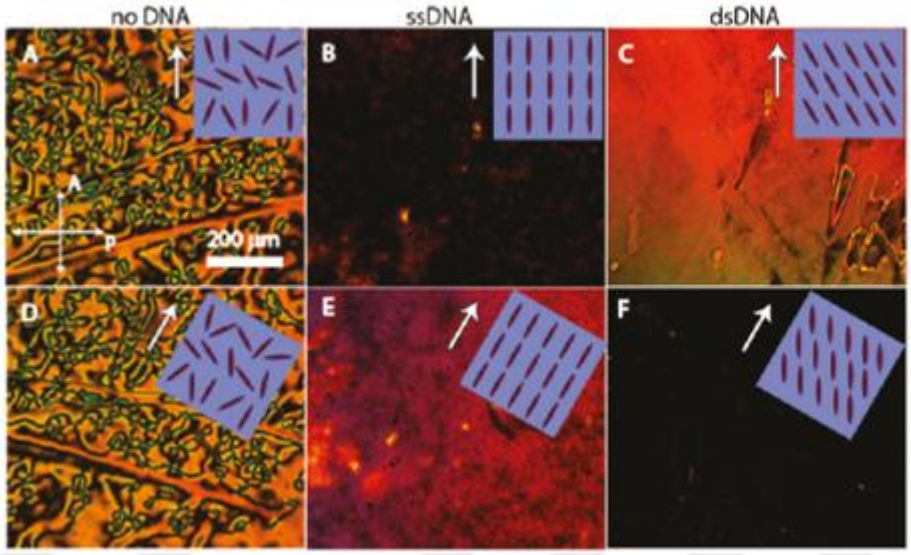

Figure 2.1 Polarized light images of LC on DNA-decorated solid surfaces. White arrow shows the direction of DNA extension on the surface. (A,D) Reference sample immersed in a buffer solution with no DNA at 0° and 30° respectively. (B,E) ssDNA decorated solid surface at 0° and 30° respectively. (C,F) dsDNA decorated surface at 0° and 30° respectively. Reprinted (adapted) with permission from Reference 25. Copyright 2011 American Chemical Society.

LC-aqueous interfaces possess advantages compared to LC-solid interfaces that favor their use in LC-sensing applications. First, mobility of the molecules at LC-aqueous interfaces is greater than LC-solid interfaces. Second, this higher mobility of the molecules enables their organization at the interface which is not possible for LC-solid interfaces. Also, LC-solid interfaces are rigid, non-deformable systems. In contrast to LC-solid interfaces, LC-aqueous interfaces can deform when they are in contact with LC molecules.[26] Due to their favorable characteristics, they are commonly used in LC-based sensors. In such a study, Brake et al. investigated the self-assembly of phospholipids at LC-aqueous interface.[12] They used a LC film exhibiting planar anchoring at the interface and exposed it to an aqueous solution of L-α-dilauroyl phosphatidylcholine (L-DLPC) in the form of vesicles. The self-assembly and organization of phospholipids at the LC-aqueous interface lead to a change in the anchoring of the LC at the interface from planar to homeotropic. As shown in Figure 2.2, the optical appearance of the LC film change from bright to dark after the decoration of the surface with phospholipids. Moreover, they examined

the binding interactions of proteins and enzymatic reactions at the phospholipid decorated interfaces with the addition of enzyme phospholipase A2(PLA2) to the aqueous phase. The specific binding of PLA2 to the interface induces a change in the anchoring of LC from homeotropic to planar.

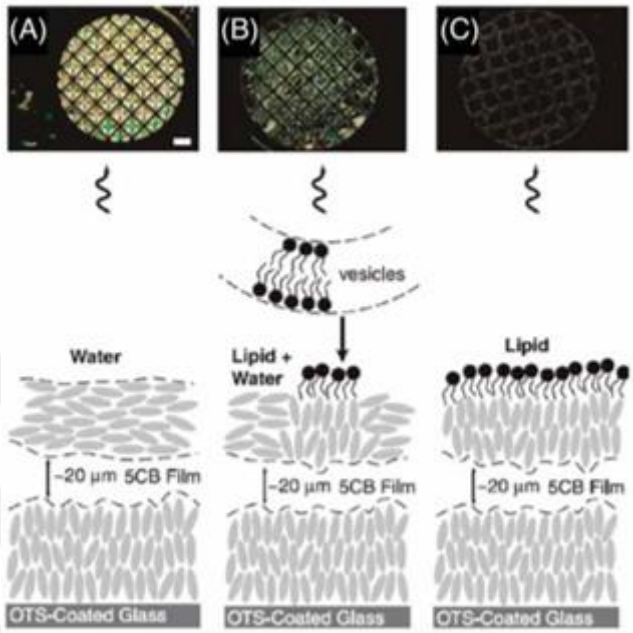

Figure 2.2 Schematic illustrations and polarized optical images of phospholipid decorated LC film. Polarized optical images of LC film (A) immediately after the addition of L-DLPC (B) after 10-20 min (C) after 2 hours of L-DLPC exposure. From Reference 12. Reprinted with permission from AAAS.

LC emulsions are preferred over other systems as they offer mobility and high sensitivity. They show a higher response than planar films of LCs due to competition between surface anchoring energy and elastic energy. Also, the initial director configuration of LC droplets determined by the surface chemistry of the droplets. Therefore, unlike LC films, they do not require any surface treatment to determine initial configurations. Owing to these properties, LC droplet interfaces are frequently used as the droplet geometries to provide well-defined configurations and strain profiles at their interfaces.[27–31]

LC droplets can be used for the detection of various molecules in solutions. Gupta et al. reported the use of LC droplets for the detection of amphiphiles.[5] They used 8

μm-sized polymer encapsulated LC droplets and demonstrated adsorbent-induced ordering transition of LC droplets with the adsorption of a surfactant (sodium dodecyl sulfate, SDS) to the LC-aqueous interface. They observed bipolar-to radial ordering transition of LC droplets with the addition of 1 mM SDS to the aqueous phase. Also, they reported the formation of equilibrium states during the anchoring transition of LC droplets with increasing concentration of SDS. Figure 1.3 shows the LC droplet configurations observed depending on the SDS concentration in the aqueous phase. As another example for the detection of molecules, Sivakumar et al reported that LC droplets can be used to sense bacteria and viruses present in the aqueous media.[17] They use gram-positive and gram-negative bacteria, enveloped and non-enveloped viruses to examine the response of LC droplets to these different types of species. They reported that LC droplets exposed to gram-negative bacteria and lipid-enveloped viruses have an ordering transition from bipolar to radial. The main reason for this transition is their similar lipid structure which transfers to the surface of LC droplets when contacting with the LC. These studies have shown that detection of such species is possible due to the change in the orientational ordering of LCs that are triggered by the adsorption of the analytes at their interface.

In addition to the studies that investigated interactions of LC with molecular species, LC interaction with micro-sized particles takes place in the literature. Musevic et al. examined the LC orientation change resulting from the confinement of microparticles in the LC medium.[32] They used silica microparticles exhibiting homeotropic anchoring in their surface distorting LC orientation around them. In this study, microparticles were confined in LC medium and introduced into a glass cell which is rubbed to have a planar anchoring, with varying LC thickness. They observed two different ordered structures forming depending on the LC orientation around the particles as shown in Figure 2.3. Microparticles formed straight chains oriented parallel to the rubbing direction when they exhibit dipolar order, in the thicker parts of the cell. In the thinner parts of the cell, microparticles exhibit quadrupolar order and causing the formation of kinked chains that align perpendicularly to the rubbing direction. The formation of these ordered structures

arises from the attractive and repulsive forces formed between particles. At the vicinity of microparticles, topological defects formed and lead to an increase in the free energy of the LC medium. Microparticles share their defects to minimize free energy and lead to an attraction force between them. Also, repulsive forces form between particles resulting from the elasticity of LC. Therefore, the balance between attractive and repulsive forces leads to the formation of two-dimensional ordered structures in the LC medium.

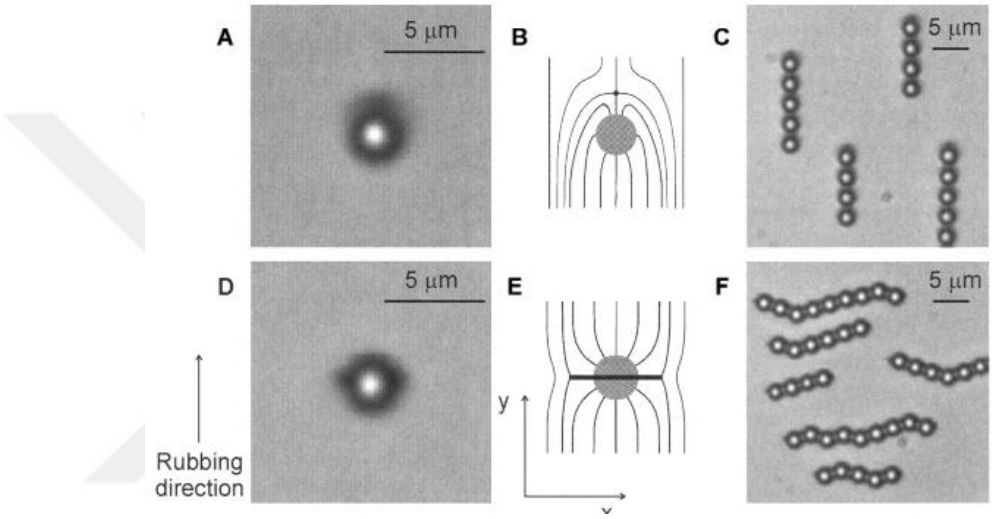

Figure 2.3 (A,D) Micrographs of dipolar and quadrupolar silica particles dispersed in LC. (B,E) Schematic illustrations of LC alignments near particles that exhibit homeotropic anchoring. (C,F) Dipolar and kinked chain structures formed in LC having a dipolar and quadrupolar symmetry respectively. From Reference 32. Reprinted with permission from AAAS.

Koeing et al. investigated the assembly of microparticles at liquid crystal-water interfaces.[18] Similar to previous study, they observe chain-like structures at the liquid crystal-water interface due to dipolar interaction between particles. Moreover, they show that the addition of surfactant to the system induces the ordering transition of LC at the interface. The LC ordering transition cause rotation of topological dipoles and changes the balance of interparticle interactions. They observed that the ordering of microparticles changes from chains to two-dimensional hexagonal arrays due to the decrease in the strength of LC-mediated long-ranged interactions as shown in

Figure 2.4. They demonstrated that the organization of microparticles at the LC-water interface can be controlled consistently with the change in LC order.

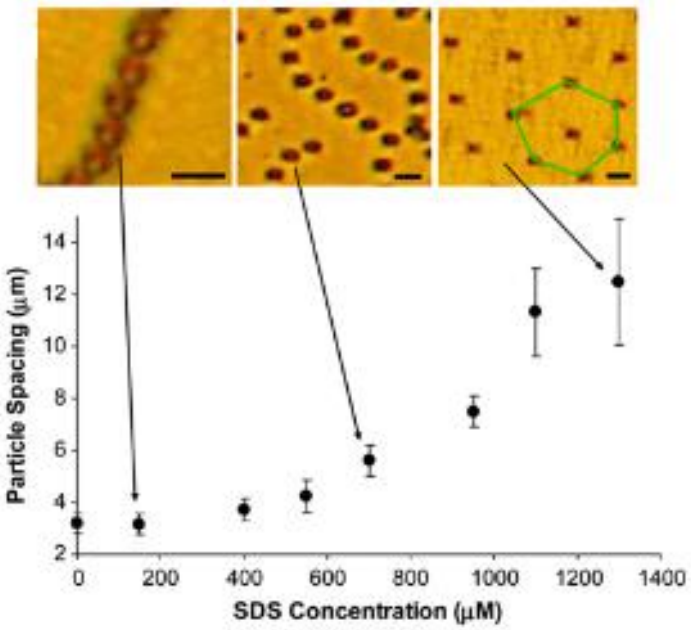

Figure 2.4 Reorganization of microparticles at the LC-water interface with the addition of surfactant to the aqueous phase. Reprinted with permission from Reference 18. Copyright 2010 National Academy of Science.

Wang et al. recently reported the adsorption of polystyrene microparticles with planar anchoring, to the surface of LC droplets and examined their organization at the LC-aqueous interface.[30] As shown in Figure 2.5B, the particles migrate to the boojum defects of the bipolar droplets and form hexagonal assemblies. Also, they investigated the importance of curvature on the direct organization of the particles at the interface. For this purpose, they adsorbed particles to the LC-aqueous interface of a planar LC film. In contrast to LC droplets, they did not observe any organization of particles in planar films due to the electrostatic repulsion between particles. Owing to the high elastic energy penalty associated with the splay elastic distortions, the organization of the particles only formed in LC droplets. This study reveals the important role of curvature on the organization of particles at the LC-aqueous interface.

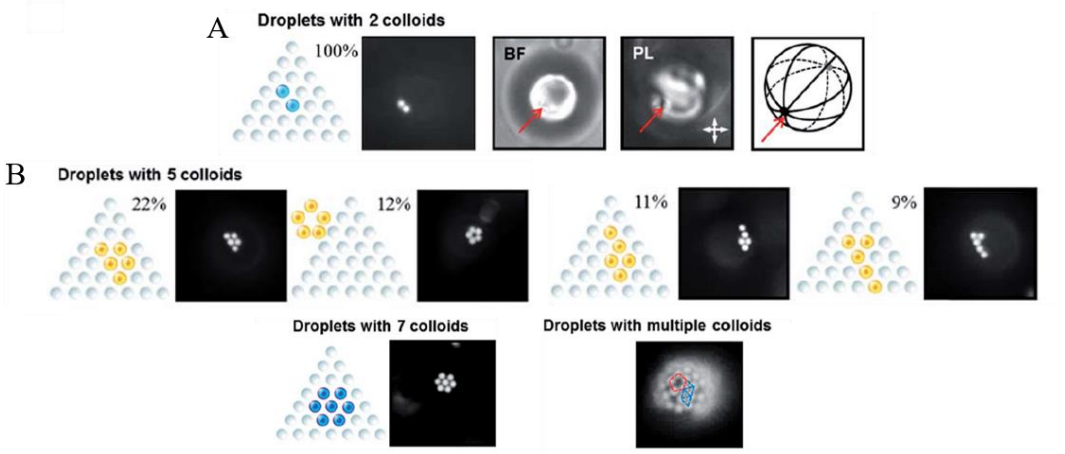

Figure 2.5 Packing arrangements observed at the pole of the droplet (A) Schematic illustration, fluorescent micrograph, bright field and polarized microscopy images of droplets with two colloids. (B) Schematic illustrations and fluorescent micrographs of the droplets with five, seven and multiple colloids. Reproduced from Ref. 30 with permission from the Royal Society of Chemistry.

Director configurations of LC droplets are determined by the balance between the key concepts of LCs. Specifically, the interplay between elastic and surface anchoring energy gives a characteristic length between 1 and 10 micrometers in which these concepts compete. Since this size range is optimal for sensing applications, preparing LC emulsions in this range is critical. The influence of droplet size on the response of LC droplets was investigated in a previous study.[7] Miller et al. examined the ordering transition of LC droplets induced by the bacterial lipopolysaccharide endotoxin.[33] As mentioned in other studies presence of 100 pg ml^{-1} endotoxin in the aqueous phase triggers the anchoring transition in LC droplets and leads to a configuration change from bipolar to radial. To investigate the influence of droplet size on LC response, they use LC droplets in the range of 2-20 µm. As shown in Figure 2.6, they observed that LC droplets in the size range between 4 and 8 µm exhibit radial configuration after the addition of 100 pg ml^{-1}. However, for the droplets with diameters larger than 10 µm, they did not observe any ordering transition. Since surface anchoring energy dominates the ordering of LC for larger droplets, the ordering transition did not observed. Furthermore, in pure water, small LC droplets exhibit radial configuration due to this scaling argument between key

concepts. They also reported that the majority of the LC droplets with a size below 2 μm maintain radial configuration consistent with the expectations.

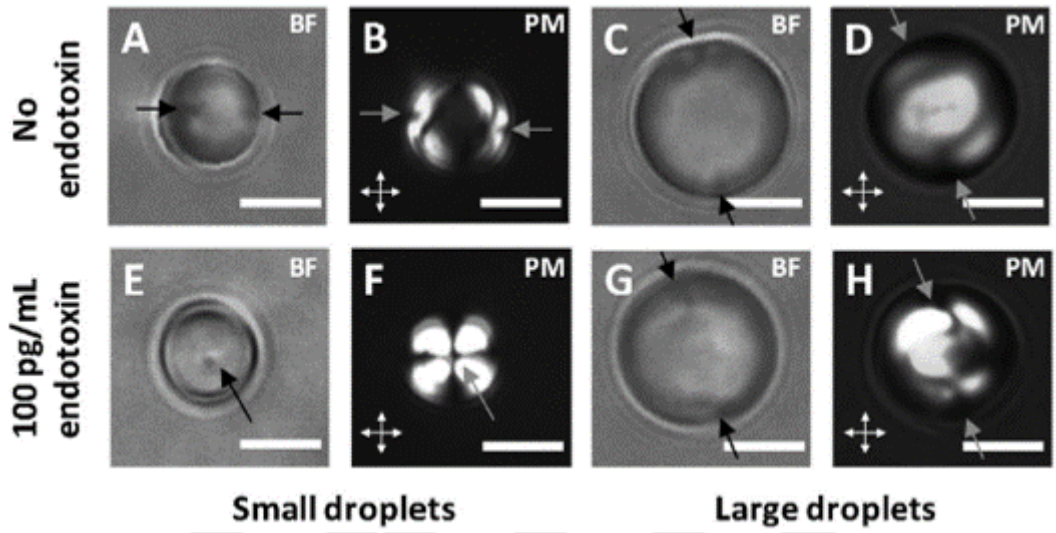

Figure 2.6 Influence of the droplet size on the response of LC droplets. Bright field and polarized micrographs of droplets exhibiting (A,B) bipolar configuration (C,D) radial configuration in PBS. Bright field and polarized micrographs of droplets exhibiting (E,F) bipolar configuration (G,H) radial configuration in the presence of 100 pg ml^{-1}endotoxin. Reproduced from Ref. 33 with permission from the Royal Society of Chemistry.

All of these studies investigated the interaction of either molecules or micro-sized particles with LCs. However, experimental studies involving LC-nanoparticle interactions do not take part in the literature. When the competition of the elastic energy and surface anchoring energy is taken into consideration, the size scale close to 1 μm is specifically important. Therefore, LC-nanoparticle interactions may differ from microparticles since their size range close to 1 μm. Previous studies examined LCs interactions with nano-sized species using simulations.

For example, a recent simulation study investigated the LC droplet configurations and the formation of ordered phases at LC droplet surfaces and revealed promising results that highlighted their technological significance. Moreno-Razo et al. decorated the surface of nanodroplets with surfactants that induce homeotropic anchoring in LCs and used LC molecules to change the organization of surfactants.[34] They observed the formation of ordered phases as circular domains or patterns at the

droplet surface as a function of the surface coverage as shown in Figure 2.7. Also, they simulated other geometries (planar, cylindrical) by decorating their surfaces with surfactants and revealed that only LC emulsions exhibit ordered phases at LC-aqueous interfaces since the elastic and surface forces on LC droplets cause the phase separation.

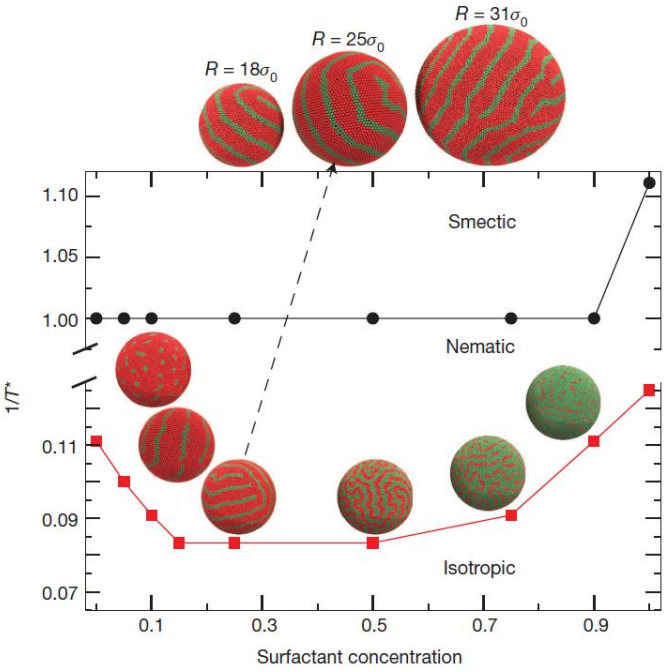

Figure 2.7 Formation of ordered phases at droplet surfaces as a function of surfactant concentration and temperature. Adapted by permission from Springer Nature Reference 34, Copyright 2012.

In a recent simulation study, Sumer et al. investigated the adsorption of nanoparticles to the LC-aqueous interface.[35] They used homogeneous and Janus particles with six different geometries to compare their organization on the surface of LC nanodroplets as shown in Figure 2.8A. Their results reveal that the shape, surface property and size of the nanoparticles are significant parameters that determine the localization of adsorbed nanoparticles at LC-water interfaces. They observed that nanoparticles with various shapes show different behaviors on LC droplets' surfaces. For example, cylindrical and cubic nanoparticles located near the equator of the LC droplet while disc-shaped nanoparticles show homogeneous distribution on droplet surface. Also,

for spherical nanoparticles, they observed a preferential localization on the boojums depend on their concentration on droplet surface. By comparing homogeneous and Janus particles of the same size and shape, they observed that nanoparticles change their preferential adsorption locations on LC droplets due to dominant LC-NP interactions. Also, they investigated the LC response upon the adsorption of nanoparticles to the LC-aqueous interface. Since nanoparticles do not penetrate into the droplet surface, their interaction with LC molecules is not strong enough to trigger a change in LC orientation. Even though they observed minor changes in the alignment of LC and shape deformations in the droplets due to the surface density of nanoparticles, these changes did not induce configuration transition in LC droplets.

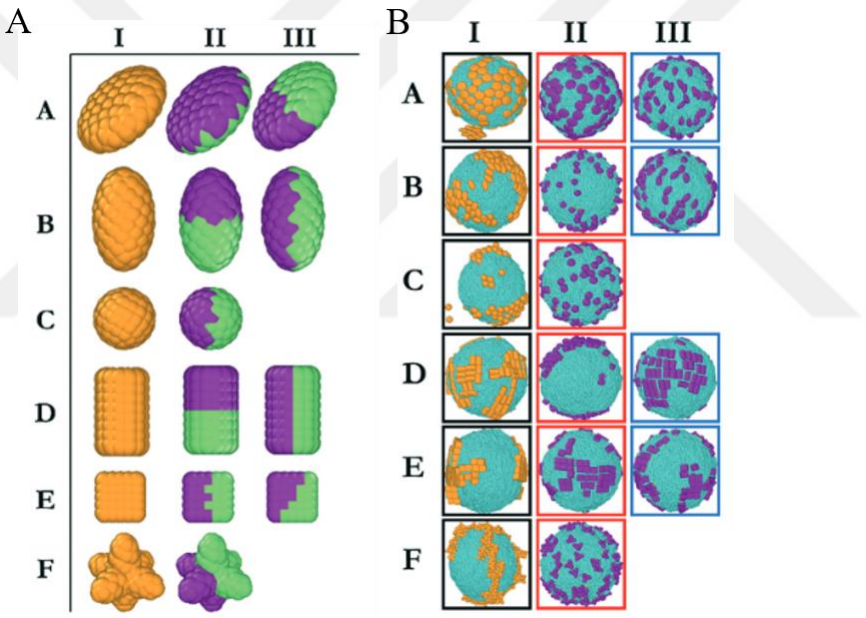

Figure 2.8 (A) Homogeneous and janus nanoparticles with different shapes used in the simulation study. (B) LC droplets obtained in simulations after the adsorption of corresponding nanoparticles on their surfaces. Reproduced from Ref. 35 with permission from the Royal Society of Chemistry.

In literature, there are many studies involving the interaction of LCs with various molecules and microparticles. However, the size range between molecular and micro-sized materials contains a broad range of species, and their detection plays a significant role in sensing applications. Furthermore, LC-nanoparticle interactions

may differ from LC-microparticle interaction sinceelastic and surface anchoring energies compete in the adsorption of nanoscale particles. So far, studies involving interactions of LCs with nano-sized materials did not go beyond simulation studies and did not include experimental observations yet. Therefore, studies on the interaction of LCs with nanoparticles must be broadened to provide insight for future technological applications.

Herein, we offer an experimental system to carry out the adsorption of nanoparticles on LC droplets. We controlled the adsorption of surface-modified nanoparticles on LC droplets and examined the response of LC droplets upon adsorption. Since nanoparticles show similarity with many species in nature regarding their sizes and surface properties, the outcomes of this study can provide fundamental knowledge for future sensing applications and novel methods for material synthesis and characterization.

CHAPTER 3

MATERIALS AND EXPERIMENTAL SECTION

3.1 Materials

Room temperature nematic mesogen, 4-cyano-4'-pentylbiphenyl (5CB), and reactive monomer 4-(3-acryloyoxy-propyloxy) benzoic acid 2-methyl-1, 4-phenylene ester (RM257) were purchased from Jiangsu Hecheng Chemical Materials Co. Ltd. (China). Photoinitiator, 2,2 dimethoxy-2-phenylacetophenone (DMPAP), anhydrous toluene, dimethyloctadecyl [3-(trimethoxysilyl) propyl] ammonium chloride (DMOAP), 3-Aminopropyltriethoxysilane (APTES, 99%), tetraethoxysilane (TEOS), ammonium hydroxide (25-30%), succinic anhydride, N,N-dimethylformamide (DMF) were purchased from Sigma-Aldrich (St. Louis, USA), and anhydrous ethanol was purchased from Isolab (Eschau, Germany).

3.2 Synthesis of Silica Nanoparticles

Silica nanoparticles were synthesized by Stöber method. TEOS used as a starting material. Mixture of 60 mL of ethanol and 3.6 mL of ammonium hydroxide were stirred for 30 min. Then 1.8 mL of TEOS was added rapidly to the solution and the mixture was stirred for 24 h at room temperature. At the end of the synthesis, the particles were collected by centrifugation and purified with ethanol for at least four times.

3.3 Preparation of DMOAP Coated Silica Nanoparticles

10 μL of DMOAP was added to 1 mL aqueous suspension of silica nanoparticles and kept in an ultrasonic bath for 15 minutes. Then, DMOAP coated nanoparticles

were removed from the medium using centrifugation (10000 rpm, 10 minutes). The supernatant was removed and replaced with ultrapure water and the particles were redispersed in the aqueous phase using an ultrasonic homogenizer. The centrifugation-redispersion steps were repeated for at least ten times to ensure the removal of the unreacted silane molecules and checked with microscopy of 5CB droplets dispersed in the final supernatant (see Results).

3.4 Preparation of Carboxylic Acid Terminated Silica Nanoparticles

Silica nanoparticles were first amino-functionalized by addition of 0.138 mL APTES to 25 mL aqueous suspension of silica nanoparticles. The mixture was stirred overnight followed by separation of nanoparticles with centrifugation (10000 rpm, 10 minutes). The supernatant was replaced with ethanol, particles were homogenized and separated using centrifugation for three times to ensure removal of the unreacted silane molecules. The nanoparticles were then redispersed in DMF and 20 mL of this solution was added dropwise to a flask containing 20 mL of 0.1 M succinic anhydride in DMF. The mixture was stirred for 24 h at room temperature. Finally, the carboxylic acid terminated silica nanoparticles were rinsed first using DMF and then using water for three times.

3.5 Preparation of Mixed-monolayer Coated Silica Nanoparticles

A mixture of 19 mL anhydrous ethanol, 1 mL of APTES and 200 μL of DMOAP were prepared. 20 mg of silica nanoparticles was dispersed in 1 mL of anhydrous ethanol and sonicated for 45 minutes. Silica dispersion was added to the mixture and solution was stirred for 1 h at 80ºC. Then the mixture was washed using ethanol for three times. The particles were then redispersed in DMF. 20 mL of this dispersion was added dropwise to a flask containing 20 mL of 0.1 M succinic anhydride in DMF. The mixture was stirred for 24 h at room temperature. Then, the mixed-

monolayer coated silica nanoparticles were rinsed first using DMF and then using water for three times.

3.6 Preparation of LC-in-water Emulsions

For the preparation of LC-in-water emulsions, 3 μL of 5CB was added to a vial containing 1 mL of aqueous silica dispersion. LC droplets were formed by mixing them using vortex mixer for 30 sec at 3000 rpm.

3.7 Preparation of Polymerized LC Droplets

RM257-5CB mesogen mixture was prepared following the methods available in the literature. A mixture of 25 wt % RM257, 75 wt % 5CB, 1 wt % photoinitiator (based on RM257 and 5CB mass) was prepared and homogenized in toluene (co-solvent) using a vortex mixer. After ensuring a homogenous mixture, toluene was evaporated under vacuum. 3 μL of the mesogen mixture was added to 1 mL of aqueous suspension of silica nanoparticles (either bare, DMOAP-coated, COOH-terminated, or mixed-monolayer coated) and mixed using a vortex mixer for 60 seconds. After formation, LC droplets were polymerized under a 365 nm UV light source for 20 min. After polymerization, unreacted mesogens were extracted by rinsing the particles at least three times with ethanol. We note here that we payed extra attention to separate the free nanoparticles during the rinsing step to prevent additional adsorption. For this, we waited for the polymerized particles to sediment naturally and collected the supernatant containing the free nanoparticles.

3.8 Optical Characterization and Measurements

Optical characterizations were carried out using a polarized optical microscope (Olympus, BX50 model). The bright field and polarized optical micrographs were

collected using a 40x objective. Size measurements of collected images were made by an open source image analysis software, Fiji ImageJ.

3.9 Characterization of Nanoparticles

The size and morphology of nanoparticles examined by X-Ray Diffraction Analysis (XRD, Rigaku Ultima-IV X-Ray Diffractometer), Fourier-Transform Infrared Spectroscopy (FTIR, Perkin Elmer Spectrum Two FTIR Spectrometer), Scanning electron microscopy (SEM, QUANTA 400F Field Emission) and Dynamic Light Scattering (DLS, Zetasizer Ultra) measurements. DLS, particle concentration and zeta potential measurements were performed using Zetasizer Ultra (Malvern instruments Ltd., US).

3.10 pH Dependent Zeta Potential Measurements of Nanoparticles

Eight different samples of water with different pH values ranging between 2 and 6 were prepared using 0.1 M HCl solution. Then, dispersions of surface-functionalized silica nanoparticles were added to the samples and zeta potential measurements were carried out using Zetasizer Ultra (Malvern instruments Ltd., US) at 25°C.

3.11 pH Dependent Zeta Potential Measurements of 5CB Droplet

LC emulsions was prepared by adding 10 μL of 5CB to 1 mL of UP water and the mixture was dispersed using a tip sonicator for 60 seconds. 2 μL of this solution was then added to 3.5 mL of water at the desired pH previously adjusted using 0.1 M HCl solution. 8 different solutions were prepared for the zeta potential measurements in the pH range of 2 and 5.8. The resulting solution was mixed using vortex mixer and zeta potential values of the samples were measured within 2 hours.

3.12 Contact Angle Measurements

Sessile drop method was used for the contact angle measurements of bare and surface modified nanoparticles with 5CB and UP water. Nanoparticles were dried on a glass slide at ambient conditions for the measurements. 163 μL/min of UP water was dropped on 4 different places on the glass slide by using Krüss DSA10-Mk2. Contact angle formed between water and the glass slide was measured immediately after contact of the water drops with the glass slide. The average value of the angles was taken. The procedure was repeated for 5CB.

3.13 Preparation of LC Droplets in Aqueous SDS Solution

SDS solutions with varying concentrations (0-1 mM) were prepared for the experiments. 3 μL of 5CB was added to a vial containing 1 mL of SDS solution. LC droplets were formed by mixing them for 10 seconds.

CHAPTER 4

RESULTS AND DISCUSSION

The methodology that we follow in this study consists of three main steps. The first step involves synthesis and surface functionalization of the nanoparticles and their characterizations. Second, preparation of the LC-in-water emulsions with adsorbed nanoparticles. Lastly, the characterization of the LC response with droplet configurations and determining controlled adsorption conditions of surface-modified nanoparticles. Figure 4.1 shows the schematic illustration of the method that was followed in this study.

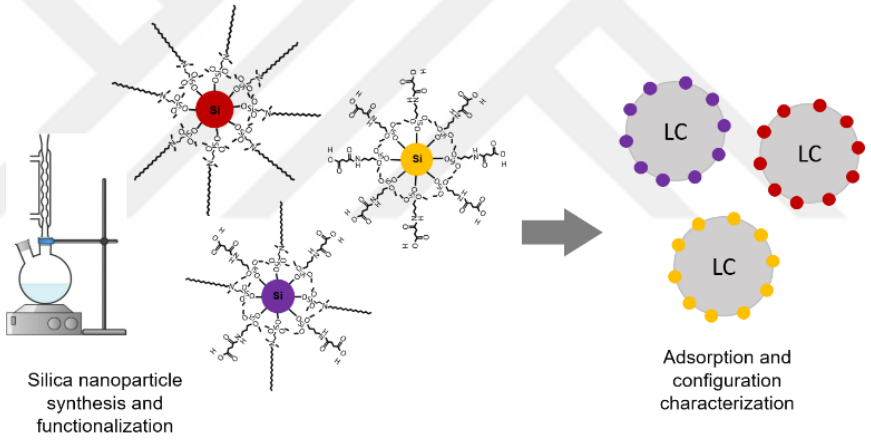

Figure 4.1 Schematic illustration of the methodology that followed in this study

4.1 Characterizations of Bare and Surface-Modified Nanoparticles

We synthesized silica nanoparticles using Stöber method[36] and performed characterizations. The XRD patterns collected from the silica nanoparticles indicate a broad peak at 2θ=23° (Figure 4.2A) and they were consistent with their counterparts in the literature.[37] The sizes of the nanoparticles were measured as 86.3 nm using DLS (Figure 4.2B), which is consistent with the average size 96.9 nm ±

11.0 nm measured from the SEM images (Figure 4.2C). The concentrations of the particles in aqueous suspensions were measured to be in the order of 10^{11} particles/mL at the end of the synthesis methods followed (Figure 4.2D).

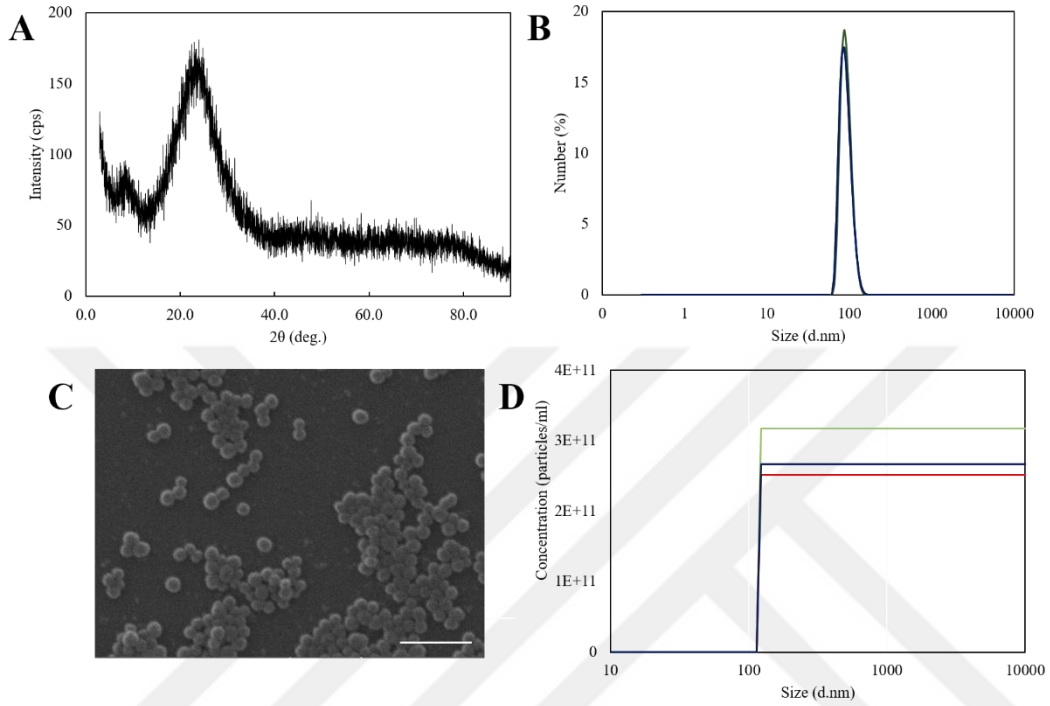

Figure 4.2 Characterizations of silica nanoparticles synthesized in this study. (A) XRD patterns of silica nanoparticles, (B) size distribution of bare silica nanoparticles obtained from DLS measurements, (C) scanning electron micrographs of bare silica nanoparticles (scale bar: 500 nm), (D) particle concentration graph of bare silica nanoparticles.

After the synthesis, we modified the surface of silica nanoparticles using either DMOAP, -COOH terminated silanes or DMOAP/COOH mixed monolayers, which possess different characteristics (hydrophobicity and charging) and mediate different anchoring conditions on LCs (either homeotropic or planar anchoring).

Firstly, we modified silica nanoparticles with DMOAP which are known to induce homeotropic anchoring of LCs, consistent with our microscopic observations of the homeotropic anchoring as shown in Figure 4.3A.[38] After coating with DMOAP, silica nanoparticles acquire hydrophobic nature resulting from the hydrocarbon tail. Consistent with this knowledge, we measured the contact angle of DMOAP-coated

silica nanoparticles with water to be 121.9 ± 4.4º. The sizes of the nanoparticles were measured as 106.6 nm using DLS (Figure 4.3B), which is consistent with the sizes of 106.1 nm ± 9.2 nm measured from the SEM images (Figure 4.3C). Zeta potential of the silica nanoparticles changed to +56.3 mV after coating with DMOAP (Figure 4.3D). Also, the concentrations of the DMOAP-coated silica nanoparticles in aqueous suspensions were measured to be in the order of 10^{10} particles/mL at the end of the surface modification as shown in Figure 4.3E.

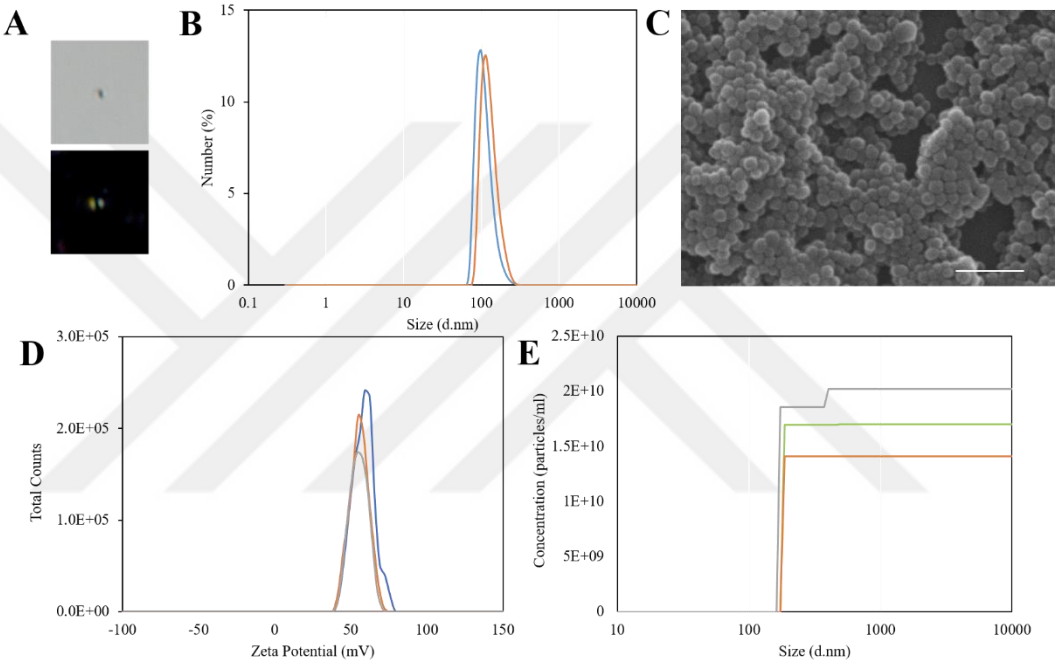

Figure 4.3 Characterizations of DMOAP-coated silica nanoparticles. (A) Brightfield and polarized optical micrographs of DMOAP-coated nanoparticles, (B) size distribution of bare silica nanoparticles obtained from DLS measurements, (C) scanning electron micrographs of DMOAP-coated silica nanoparticles (scale bar: 500 nm), (D) zeta potential measurements of DMOAP-coated silica nanoparticles in water, (E) particle concentration graph of DMOAP-coated silica nanoparticles.

Secondly, the nanoparticles were functionalized with -COOH-terminated silane groups that provide nanoparticles a pH dependent electrical charge, hydrophilic nature, and a planar anchoring of LCs.[39] Surface functionalization of nanoparticles with -COOH terminated-silane groups was carried out in two steps. Firstly, amine groups were introduced to the surface of silica nanoparticles by treatment of

nanoparticles with APTES. Secondly, amine groups were converted into -COOH groups by a ring-opening elongation reaction with succinic anhydride.[40] The sequential surface modification of silica nanoparticles with amine and carboxylic acid groups was confirmed by different characterization methods. FT-IR spectra given in Figure 4.4A shows the spectra collected during the surface modification of carboxylic acid terminated silica nanoparticles that is consistent with the desired functionalization.[41] Also, the change in surface charge and size of the nanoparticles confirmed the surface modification. Zeta potential of the bare silica nanoparticles changed from -67 mV to 18.5 mV after surface modification of nanoparticles with APTES groups. Then, due to the presence of -COOH-terminated silane groups, zeta potential of the nanoparticles changed to -58 mV at the end of the synthesis methods followed. (Figure 4.4B). Similarly, the average diameter of the bare silica nanoparticles was measured as 88.4 ± 3.0 nm and increased to 122.3 ± 2.5 nm after surface modification with -COOH terminated silane groups as shown in Figure 4.4C. Contact angle of water on -COOH-terminated nanoparticles were measured as 17.9 ± 2.2º, which confirms their hydrophilicity, and our microscopy observations supported the planar LC anchoring (Figure 4.4D). Also, the concentrations of the particles in aqueous suspensions were measured to be in the order of 10^{10} particles/mL at the end of the surface modification methods followed (Figure 4.4E).

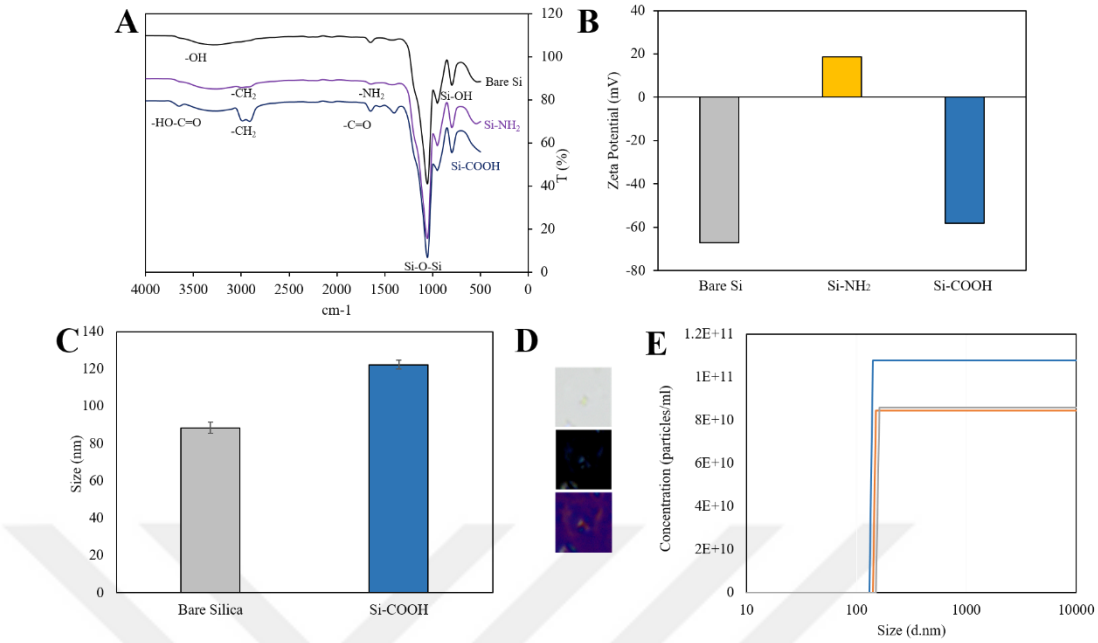

Figure 4.4 Characterizations of -COOH terminated silica nanoparticles. (A) FT-IR spectra of bare, APTES-functionalized, and -COOH terminated silica nanoparticles. (B) zeta potential measurements of bare, APTES functionalized and -COOH functionalized silica nanoparticles in water, (C) size measurements of bare and -COOH functionalized silica nanoparticles obtained from DLS measurements, (D) brightfield and polarized optical micrographs of -COOH terminated silica nanoparticles, (E) particle concentration graph of -COOH terminated silica nanoparticles.

Lastly, we modified the nanoparticle surfaces using combination of DMOAP and -COOH-terminated silanes to obtain a mixed-monolayer on the particle surface and examine the surface property-dependent change in LC droplet response. Size and zeta potential measurements were used to confirm the surface functionalization of silica nanoparticles. The average diameter of the bare silica nanoparticles measured as 113 ± 2.83 nm and increased to 154 ± 1.0 nm after surface modification with -COOH/DMOAP terminated silane groups (Figure 4.5A). Similarly, zeta potential of the bare silica nanoparticles changed from -29.0 ± 13.8 mV to 39.2 ± 18.3 mV after surface modification of nanoparticles with APTES and DMOAP groups. Then, zeta potential of the nanoparticles changed to -31.8 ± 3.0 mV at the end of the synthesis methods followed (Figure 4.5B). The contact angle of water on nanoparticles with DMOAP/COOH mixed monolayer was measured as 40.8 ± 6.1°. The concentrations

of the particles in aqueous suspensions were measured to be in the order of 10^{10} particles/mL at the end of the surface modification (Figure 4.5C).

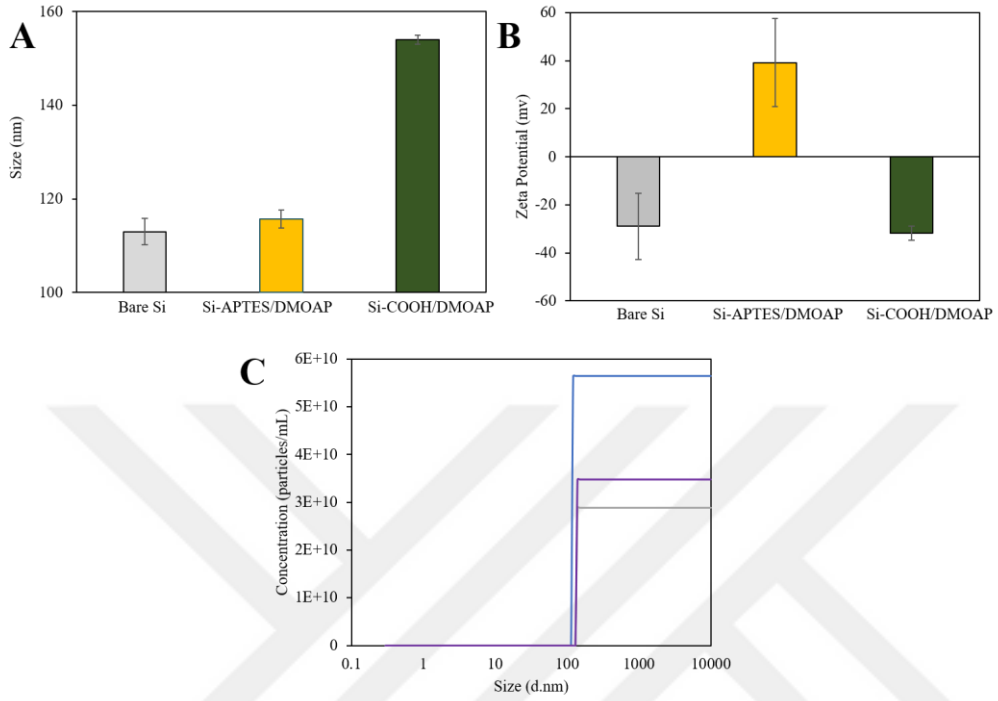

Figure 4.5 Characterizations of -COOH/DMOAP terminated silica nanoparticles. (A) Size measurements of bare, APTES/DMOAP functionalized and-COOH/DMOAP functionalized silica nanoparticles obtained from DLS measurements (B) zeta potential measurements of bare, APTES/DMOAP functionalized and COOH/DMOAP functionalized silica nanoparticles in water, (C) particle concentration graph of -COOH/DMOAP terminated silica nanoparticles.

Beyond these characterizations, we also measured the contact angle of 5CB on DMOAP-coated particles to be 17.1 ± 1.5º, on -COOH terminated silane coated nanoparticles to be 22.6 ± 0.8º, and on -COOH/DMOAP mixed monolayer-coated nanoparticles to be 25.4 ± 2.6º. We concluded 5CB to wet the surfaces of the nanoparticles. Contact angle measurements of 5CB and water on bare and surface modified nanoparticles shown in Figure 4.6.

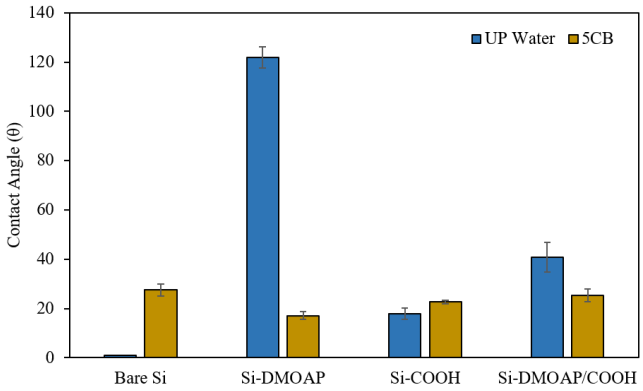

Figure 4.6 Contact angle measurements of 5CB and water on bare and surface modified nanoparticles

To investigate the effect of nanoparticle size on the response of LC droplets, we synthesized ~50 nm-sized silica nanoparticles using Stöber method. The sizes of the bare nanoparticles were measured as 49.4 nm using DLS. After the synthesis, we modified the surface of silica nanoparticles using either DMOAP and -COOH terminated silane groups. The sizes of the DMOAP-coated and -COOH terminated nanoparticles were measured as 111.3 nm and 114 nm respectively (Figure 4.7A). Zeta potential of the nanoparticles changed from -46 mV to 20.9 mV after coating with DMOAP and to -16.9 mV after -COOH functionalization (Figure 4.7B). The concentrations of the particles in aqueous suspensions were measured to be in the order of 10^9 particles/mL for both DMOAP-coated and -COOH terminated nanoparticles. Figure 4.7 shows the characterizations performed for smaller silica nanoparticles.

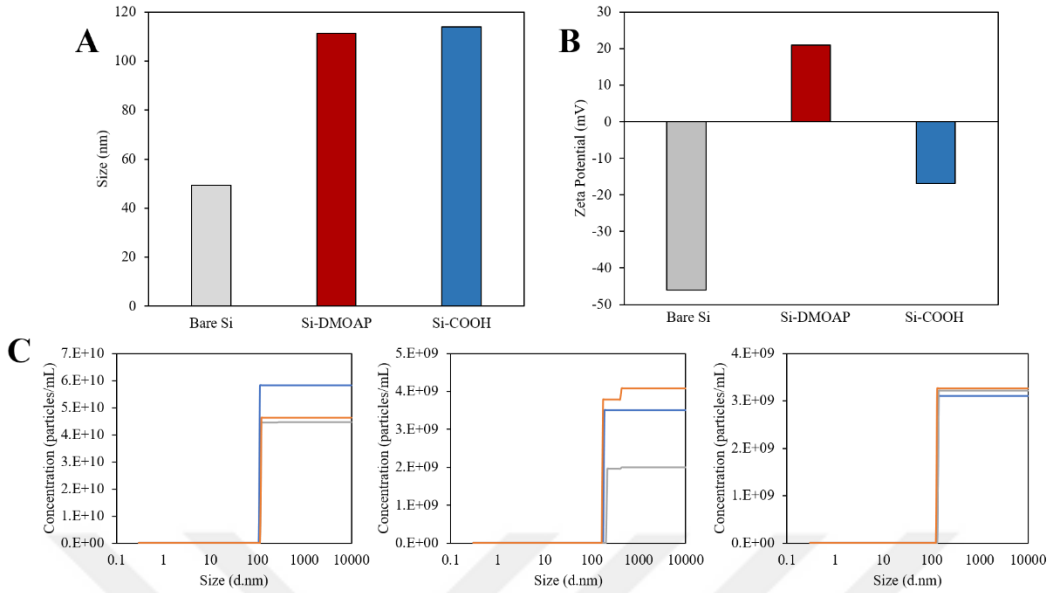

Figure 4.7 Characterizations of 50nm-sized bare and surface functionalized silica nanoparticles. (A) size measurements of bare, DMOAP-coated and -COOH functionalized silica nanoparticles obtained from DLS measurements, (B) zeta potential measurements of bare, DMOAP-coated and -COOH functionalized silica nanoparticles in water, (C) particle concentration graphs of bare, DMOAP-coated and -COOH terminated silica nanoparticles respectively.

4.2 Preparation of LC-in-water Emulsions and Their Characterizations

For the interest of the nanoparticle adsorption induced ordering transitions in LC droplets, we prepared droplets of diameters in the range of 1-10 μm with a number average size of 4.9 ± 0.9 μm as shown in Figure 4.8A. Within this range, the configuration distribution of the 5CB droplets were found to be 96.7 ± 2.7% bipolar when dispersed in pure water, which is characterized by two boojum defects at the two opposite poles of the droplets. The observation of this configuration is consistent with the planar anchoring of 5CB at their interfaces with water.[1,5,26] We also note that the configuration distribution of the bare 5CB droplets in water is not dependent on the pH of the aqueous phase down to pH=3, consistent with the literature.[42]

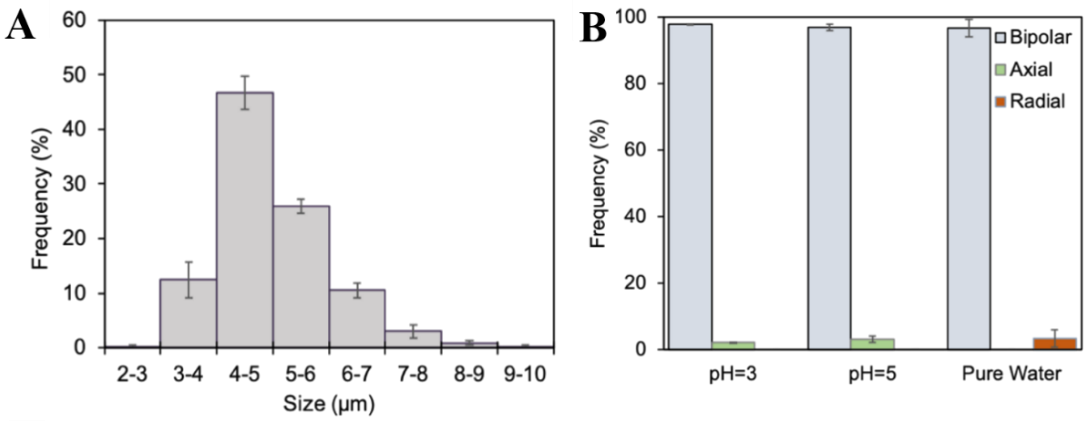

Figure 4.8 (A) Size distribution graph of LC droplets, (B) Configuration distributions of LC droplets at pH 3, pH 5 and in pure water (measured as pH 5.9)

For our interest to observe 5CB droplet configurations experimentally, we performed experiments using SDS at different concentrations. With the adsorption of SDS at the LC-aqueous interface, configuration transition took place due to the change in the anchoring from tangential to homeotropic. To test this, we performed experiments at six different SDS concentrations. In the absence of SDS in water, 5CB droplets maintained bipolar configuration as we have mentioned before. With increasing SDS concentration in water, we observed a decrease in the total frequency of bipolar configurations and an increase in the frequency of radial configurations. Between 0 and 1 mM of SDS concentrations, we observed different equilibrium states of 5CB droplets as axial and preradial consistent with the literature.[5] Representative 5CB droplet configurations observed during experiments and their configuration distribution depending on SDS concentration in the solution shown in Figure 4.9.

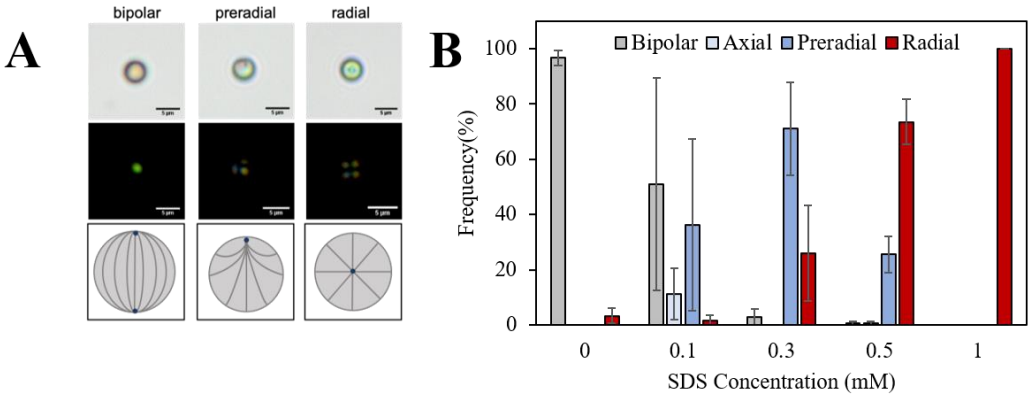

Figure 4.9 (A) Brightfield (top), polarized light (middle) micrographs and the configuration sketches (bottom) of the 5CB droplets exposed to SDS at different concentrations, (B) Configuration distributions of LC droplets at different SDS concentrations.

4.3 Adsorption of Nanoparticles to the LC-Aqueous Interfaces and Characterization of the LC Droplet Response

One of our goals in this study is to investigate the response of the LC droplets to the adsorption of the nanoparticles from aqueous phase. For this purpose, we first performed experiments with bare silica nanoparticles and quantified the response of 5CB droplets upon adsorption of the nanoparticles. The adsorption of nanoparticles on interfaces is highly dependent on the charge effects and surface characteristics of the particles. The literature reports indicate negative zeta potential of the LC droplets.[43] Similarly, bare silica nanoparticles exhibit a negative zeta potential of -49.6 ± 0.8 mV. Therefore, due to the hydrophilic nature and negative surface charge of bare silica nanoparticles, adsorption of silica nanoparticles on the LC-water interface is not expected. In the experiments, 5CB droplets maintained 74.1% bipolar configuration upon exposure to bare silica nanoparticles (Figure 4.10A). The observation of this configuration is the same with the configuration of bare 5CB droplets in pure water. To investigate the presence of nanoparticles on LC-water interface, we performed adsorption experiments with nematic mixtures of the reactive mesogen (RM257) in 5CB (25% by weight) and polymerized the reactive mesogens after adsorption of the nanoparticles. During this treatment, we paid

attention to prevent additional adsorption of nanoparticles in the solution. Therefore, we naturally sedimented polymerized LC droplets and change the supernatant with fresh water for three times. In the SEM images, we did not observe any coverage of nanoparticles at the droplet interfaces which confirms the observations from the response tests. In the absence of adsorbed nanoparticles, the rough surface feature of bare LC droplets was observed in the SEM images consistent with the literature.[44] The representative SEM image of the polymerized droplets shown in Figure 4.10B.

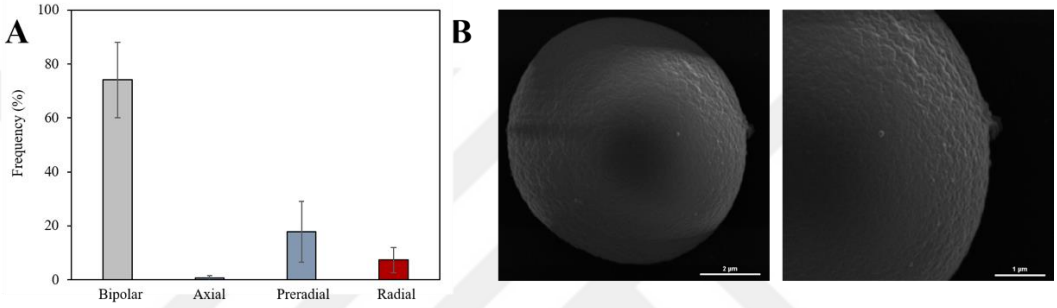

Figure 4.10 (A) Configuration distributions of LC droplets present in suspensions of bare silica nanoparticles, (B) Scanning electron micrograph of polymerized LC droplets that was exposed to suspension of bare silica nanoparticles (scale bar:2μm).

Secondly, we performed experiments with DMOAP-coated nanoparticles and quantified the response of 5CB droplets upon adsorption of the nanoparticles. 5CB droplets maintained either radial or preradial configurations upon exposure to DMOAP-coated nanoparticles with concentrations of 1.7 x 10^{10} particles/mL as shown in Figure 4.11A. These configurations are indicative of the homeotropic (or slightly tilted) anchoring of 5CB at the interface of the LC and nanoparticles, which is consistent with the homeotropic surface anchoring of the DMOAP-coated silica surfaces.[38] Also, we performed control experiments with the supernatant of the DMOAP-coated particles (i.e. everything except the particles) and observed bipolar configuration in the 84.4 ± 4.0% of the droplets supporting that the resulting configurations were due to the presence of the nanoparticles in the suspension (Figure 4.11B).

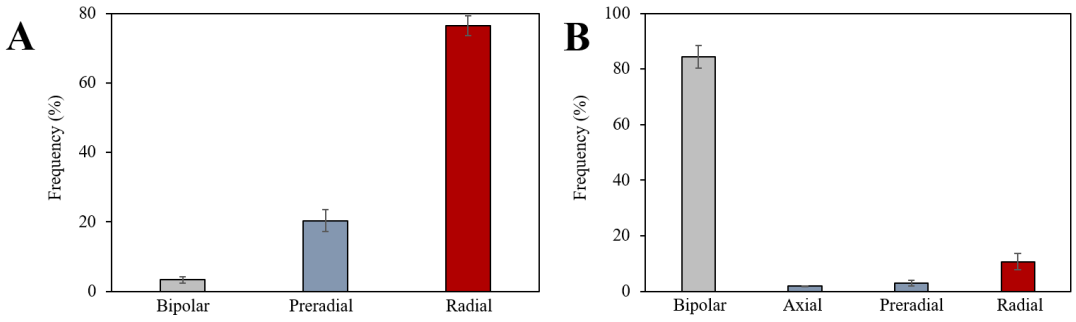

Figure 4.11 (A) Configuration distributions of LC droplets present in suspensions of DMOAP-coated silica nanoparticles, (B) Configuration distributions of LC droplets present in the supernatant of the DMOAP-coated particles.

Then, we performed experiments with suspensions of different DMOAP-coated particle concentrations. With decreasing concentration of the nanoparticles, we observed a decrease in the total frequency of the preradial and radial configurations. The droplets exhibited either preradial or radial configurations in average of 90.1 ± 6.4% of the total number for nanoparticle concentrations of 1.7 x 10^9 particles/mL whereas the frequency of the same configurations decreased to 6.9 ± 7.1% for concentration of 1.7 x 10^8 particles/mL (Figure 4.12). We make two observations based on these results. First, we observed three different configurations for the droplets upon exposure to DMOAP-coated particles. When compared to the droplet configurations reported in the literature, axial or escaped radial configurations were also observed in 5CB droplets of this size range at intermediate coverage of the droplets with surfactants.[5] We reasoned that the absence of these intermediate configurations was due to the chemical heterogeneity at the LC-water interface caused by the adsorption of the particles, therefore the resulting "defect pinning" of the point defect close to the LC-water interface. Second, a strong dependence of the droplet configurations on the concentrations of the DMOAP-coated nanoparticles is evident in Figure 4.12. This result is consistent with the estimations based on the interfacial coverage of the droplets. When estimated a monolayer of close packed nanoparticles on the LC-water interface of the emulsion to be in the order of 10^{10} particles/mL. Considering the high hydrophobicity of the DMOAP-coated nanoparticles, the particles initially present in the aqueous medium were expected to

localize at the LC-water interface. Thus, exposure of the droplets to nanoparticle concentrations below the monolayer of random close packing would result in partial coverage of the interfaces, which is expected to result in a decreased frequency of their radial configurations supporting the critical concentration that we observe in our experiments. This phenomenon also explains the highest frequency of the preradial configurations at the intermediate nanoparticle concentrations we study.

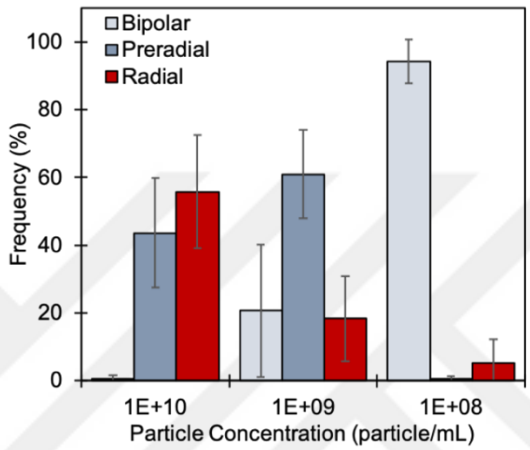

Figure 4.12 Configuration distributions of 5CB droplets present in suspensions of different DMOAP-coated particle concentrations.

For our interest of the imaging of the silica nanoparticles at the interfaces of the droplets, we performed adsorption experiments with nematic mixtures of the reactive mesogen RM257 in 5CB (25% by weight) and polymerized the reactive mesogens after adsorption of the nanoparticles. We note here that this treatment required special attention (*i*) to prevent additional adsorption of particles to the LC-water interfaces during polymerization and extraction steps and (*ii*) to prevent desorption of the particles during dilution steps. To prevent further adsorption during separation of the polymerized droplets from free nanoparticles, we naturally sedimented the polymerized droplets for at least three times and replaced the supernatant with fresh water. Then, we extracted the unreacted part of the droplets for at least three times with ethanol. When the adsorption energy of the particles on the LC-water interfaces was calculated using;

$$E = \pi a^2 \lambda (1 + \cos(\alpha))^2 \qquad \text{(Equation 3)}$$

where a is the nanoparticle radius (~50 nm), λ is the surface tension (0.03 N/m), and α is the interfacial contact angle of the LC-water interface (~40º), the adsorption energy was found as ~10^5 k_BT indicative of an irreversible adsorption of the particles to the LC-water interfaces. We also supported the prediction of the irreversible adsorption of the particles to the LC-water interfaces with dilution experiments of the droplets that were initially exposed to suspensions of 10^{10} particles/mL. Consistent with the irreversible adsorption of the nanoparticles, we did not observe a significant change of the configuration distribution of the 5CB droplets even after dilution of the aqueous phase up to 100 times as shown in Figure 4.13, which would otherwise result in 96.7 ± 2.7% bipolar configuration.

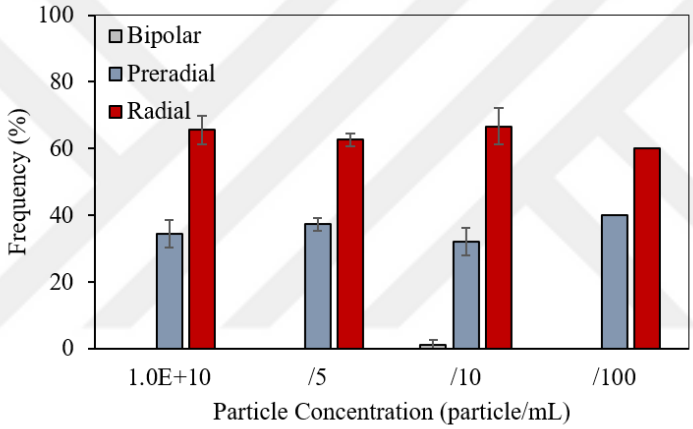

Figure 4.13 Configuration distributions of 5CB droplets initially dispersed in suspensions of DMOAP-coated nanoparticles after dilution with water.

Representative SEM images of the polymerized droplets are shown in Figure 4.14. As highlighted above, we did not observe features on the surfaces of the droplets that would be considered as the desorption of the particles from their surfaces. The images show that the droplets incubated in nanoparticles suspensions with concentrations of 10^{10} particles/mL resulted in almost a monolayer coverage of the particles at their interfaces. Decrease in the concentrations of the particles in the suspension were shown to result in a decrease in the surface coverage of the particles at the droplet interfaces as expected. More importantly, the nanoparticles adsorbed at the interfaces of the droplets were observed to form clusters of sizes in the scale

of micrometers, rather than single dispersion of the particles which is expected due to the strong hydrophobicity of the DMOAP-coated nanoparticles. These aggregates were observed to induce preradial configurations as a result of the "defect pinning", whose signatures were observed as the anisotropic tear-drop shapes of the polymerized droplets with the cusp edge corresponding to the location of the nanoparticle aggregates (shown in yellow arrow in Figure 4.14B). [45]

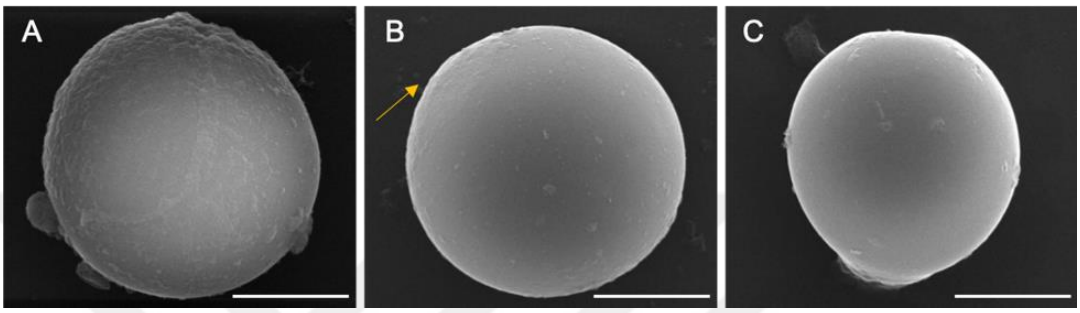

Figure 4.14 Scanning electron micrographs of polymerized LC droplets. The droplets were exposed to suspension of DMOAP-coated silica nanoparticles with concentrations of (A)10^{10}, (B)10^{9}, and (C)10^{8} particles/mL before polymerization. Scale bars: 5 μm.

One of our goals in this study is to determine controlled adsorption conditions of surface-modified nanoparticles. Since the adsorption of nanoparticles on interfaces is highly dependent on the charge effects and surface characteristics of the particles, before investigating the controlled adsorption conditions, we first focused on the charge of the LC droplets and surface modified nanoparticles. The literature reports indicate negative zeta potential of the LC droplets, which is dependent on the pH of the medium.[43] We confirmed the pH-dependent zeta potential of LC droplets with measurements in the range of +7.5 ± 23.6 mV at pH = 2 to -56.1 ± 7.0 mV at pH = 5.9, and also measured that of the surface-modified nanoparticles as shown in Figure 4.15.

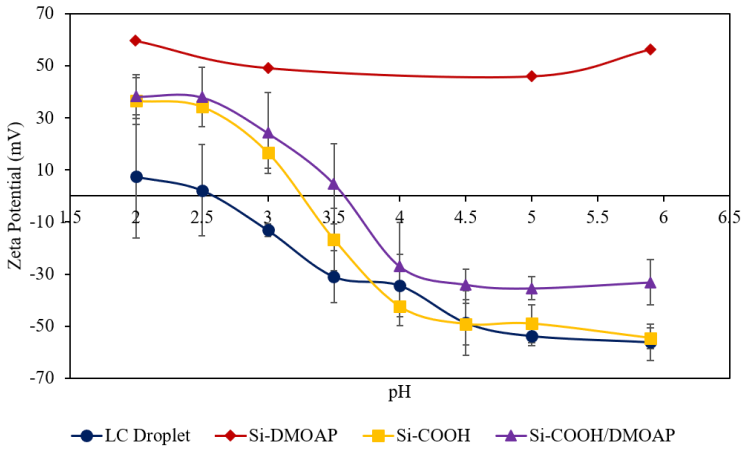

Figure 4.15 Zeta potential as a function of pH of the LC droplets and surface modified silica nanoparticles.

Bare silica nanoparticles exhibit a zeta potential of -49.6 ± 0.8 mV. After functionalization of the nanoparticles with DMOAP, their zeta potential was measured to be +56.3 ± 1.6 mV. This strong positive zeta potential value also promoted the adsorption of the DMOAP-coated particles to the droplets as reported above. DMOAP-coated particles do not exhibit a pH-dependent zeta potential. Therefore, the adsorption of DMOAP-coated nanoparticles to the LC-water interface is not affected by the pH of the aqueous medium. To demonstrate this, we performed adsorption experiments at pH of 2, 3, and 5. As can be seen in Figure 4.16A, the pH of the aqueous nanoparticle suspension did not influence the configuration distribution of 5CB droplets dispersed in the medium. We also performed electron microscopy of the polymerized 5CB droplets after the adsorption of the nanoparticles at the three different pH conditions to image the nanoparticles. The droplets exhibited a full coverage of the particles at their interfaces as shown in Figure 4.16(B-D). Therefore, changing pH of the medium did not induce any change in the surface coverage of the particles at the droplet interfaces as expected.

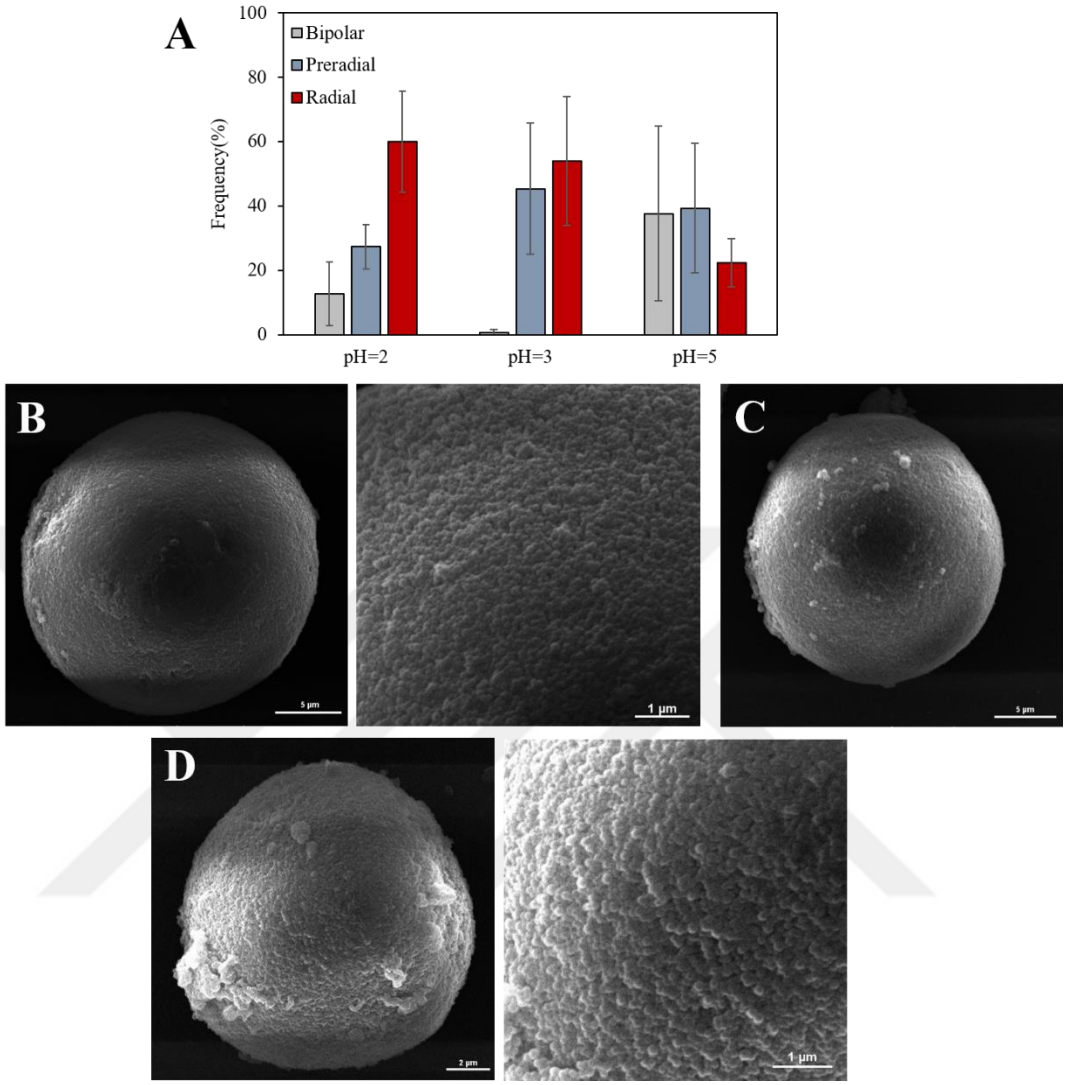

Figure 4.16 (A) Configuration distribution of 5CB droplets dispersed in suspensions of DMOAP-coated silica nanoparticles at different pH, (B-D) Scanning electron micrographs of polymerized LC droplets after contacting with suspensions of DMOAP-coated silica nanoparticles at pH of 2, 3 and 5 respectively.

Then, we performed experiments with -COOH-terminated silica nanoparticles and quantified the response of 5CB droplets upon adsorption of the nanoparticles. 5CB droplets exhibited bipolar configuration in average of 85.0 ± 6.9% upon exposure to -COOH-terminated particles with concentrations of 9.3×10^{10} particles/mL as shown in Figure 4.17A. Since the configuration distribution of the droplets are similar with the bare droplets in water, we also performed electron microscopy of the polymerized 5CB droplets after the adsorption of the nanoparticles to image the

presence of the nanoparticles. -COOH terminated silica nanoparticles exhibit a zeta potential of -54.6 ± 4.0 mV in pure water (pH=5.9). Similarly, LC droplets have a zeta potential of -56.1 ± 7.0 mV in pure water. Since both particles and droplets are negatively charged, the charge repulsion cause lower adsorption of the particles to the surfaces of the droplets. By using electron microscopy, we observed that LC droplets exhibited a very low coverage of the particles as expected (Figure 4.17B).

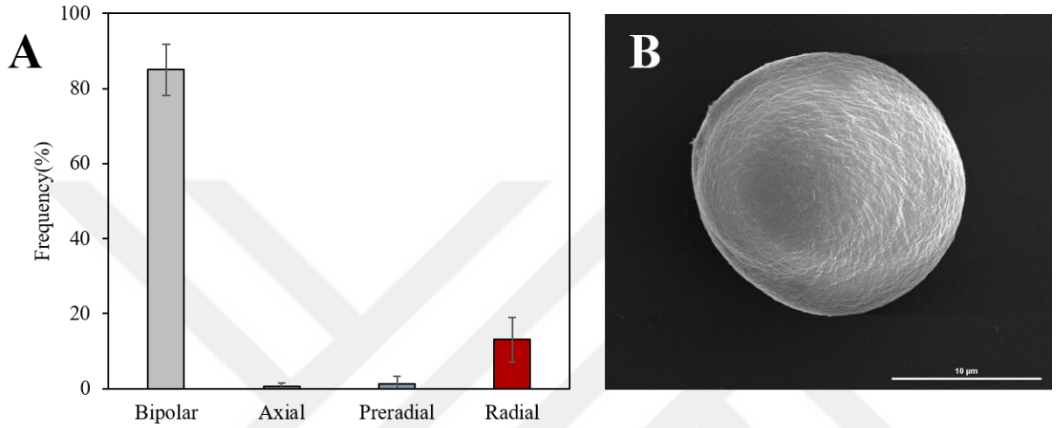

Figure 4.17 (A) Configuration distributions of LC droplets present in suspensions of COOH-terminated silica nanoparticles, (B) scanning electron micrograph of the polymerized LC droplet that was exposed to suspension of COOH-terminated silica nanoparticles.

The nanoparticles functionalized with -COOH-terminated silanes maintained a pH-dependent zeta potential due to the presence of the weak acid groups. The isoelectric point of the COOH-terminated silica nanoparticles were found to be at pH = ~3.3, consistent with the carboxylic acid terminated surface functionality. Previous studies reported the isoelectric point of COOH-terminated nanoparticles.[40,46,47] We specified the isoelectric point of -COOH terminated nanoparticles from three independent measurements conducted with three different batch of nanoparticles. Our measurement is consistent with the studies reporting isoelectric point of COOH-terminated nanoparticles as pH>3.[46,47] We thought that the difference in the measurements may result from the dissimilarity between the synthesis or surface functionalization procedures. Such pH-dependent measurements of the zeta potential

of the nanoparticles provided opportunity to control the adsorption of the particles to droplet interfaces.

After measuring the pH-dependent zeta potential of the -COOH functionalized particles and the droplets, we took advantage of their pH-dependent charges for the controlled adsorption of the nanoparticles. We chose pH of 2, 3, and 5 for the adsorption experiments to maintain droplets and particles with both positive, opposite and both negative charges, respectively. The results of such experiments are shown in Figure 4.18. As seen in Figure 4.18A, the pH of the aqueous nanoparticle suspension did not influence the configuration distribution of 5CB droplets dispersed in the medium. Since the configuration distribution of the droplets are of similar statistics with the bare droplets as shown in Figure 4.8B, we also performed electron microscopy of the polymerized 5CB droplets after the adsorption of the nanoparticles at the three different pH conditions to image the presence of the nanoparticles. As shown in Figure 4.18C, for the experiment conditions with droplets and nanoparticles are of the same charge (as in pH = 2 and 5), the droplets exhibited a low coverage of the particles. However, for pH = 3, the droplet surfaces were observed to be covered with a close packed monolayer of the nanoparticles. We here note also that the wrinkling of the particle monolayer observed on the droplet interfaces at pH = 3 was resulted from the shrinkage of the polymerized droplets after the extraction of the unreacted mesogens, which was detailly documented in the literature(Figure 4.18B).[44,45,48–50] When combined with the experiments performed for the configuration of 5CB droplets, we concluded that (*i*) the control of the adsorption of the -COOH-terminated particles on LC droplet interfaces can be done by tuning the pH of the suspension medium, and (*ii*) the COOH-terminated particles promotes planar anchoring of LC on their interfaces.

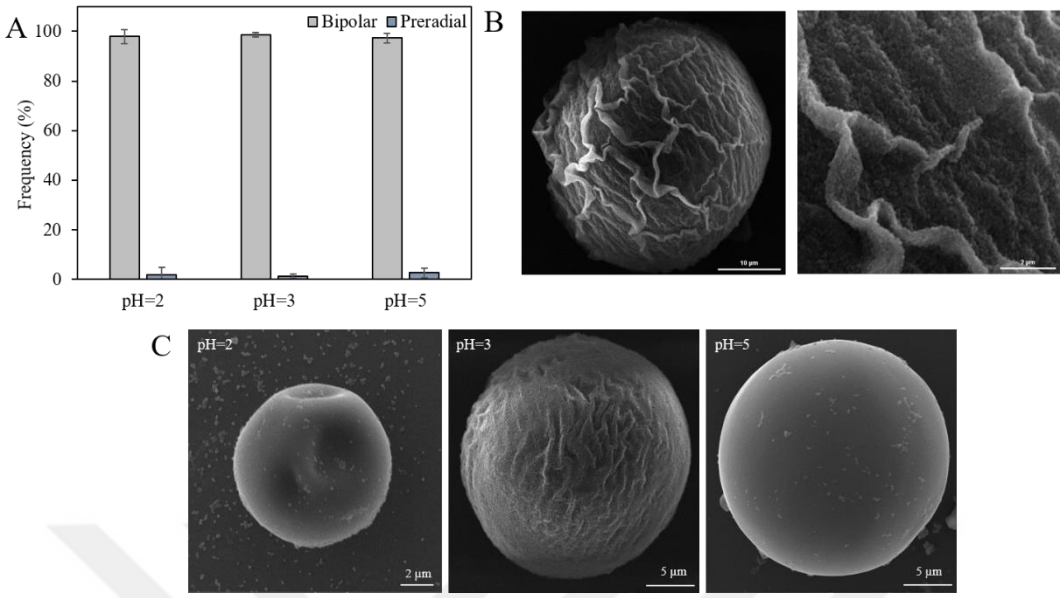

Figure 4.18 (A) Configuration distribution of 5CB droplets dispersed in suspensions of COOH-terminated silica nanoparticles at different pH, (B) scanning electron micrographs of polymerized LC droplets after contacting with suspensions of COOH-terminated silica nanoparticles at pH = 3, (C) scanning electron micrographs of polymerized LC droplets after contacting with suspensions of COOH-terminated silica nanoparticles at different pH.

We also performed experiments by changing COOH-terminated particle concentration in the suspension at pH=3. 5CB droplets maintain bipolar configuration upon exposure to -COOH-terminated particles at different concentrations as shown in Figure 4.19A. We also performed electron microscopy of the polymerized 5CB droplets after the adsorption of the nanoparticles with different concentrations to image the density of the adsorbed nanoparticles on droplet surface (Figure 4.19(B-D)). Decrease in the concentrations of the particles in the suspension causes a decrease in the surface coverage of the particles at the droplet interfaces as expected.

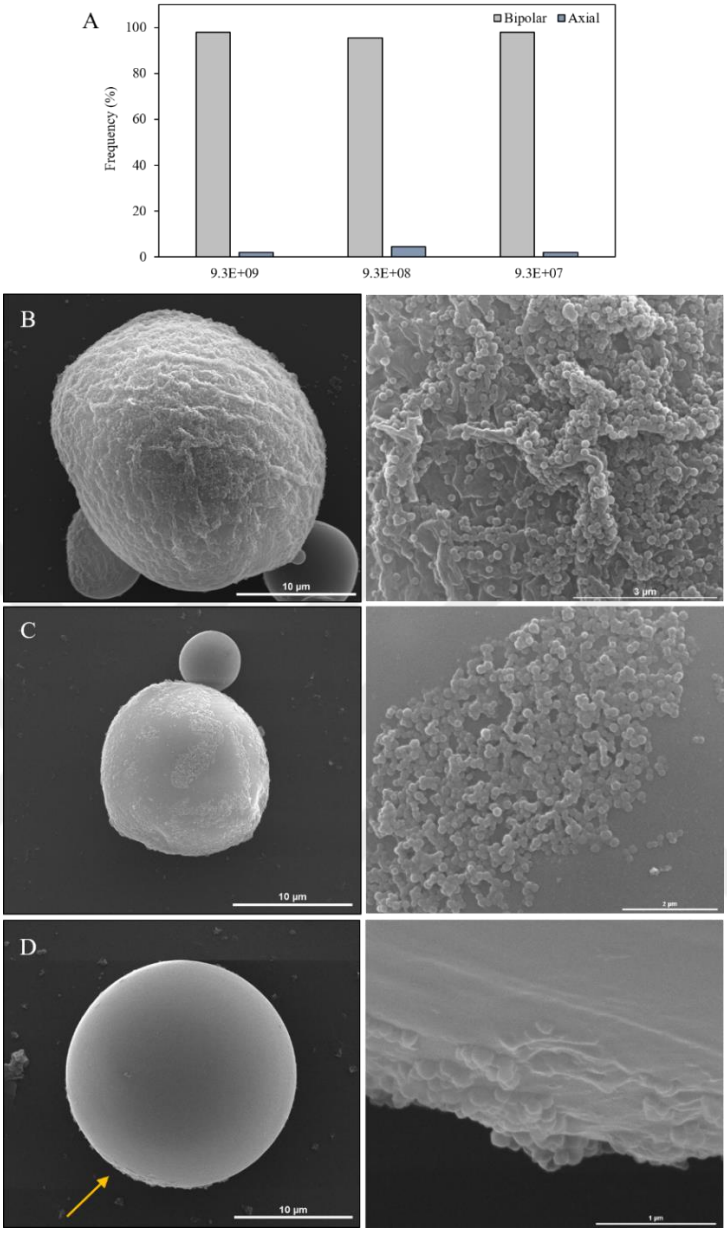

Figure 4.19 (A) Configuration distributions of 5CB droplets present in suspensions of different -COOH terminated particle concentrations (B-D) scanning electron micrographs of polymerized LC droplets. The droplets were exposed to suspension of COOH-terminated silica nanoparticles with concentrations of (B) 10^9, (C) 10^8, and (D) 10^7 particles/mL before polymerization.

In the last part of this study, we performed experiments on the adsorption of the nanoparticles functionalized with mixed monolayers of -COOH-terminated silanes and DMOAP. We observed a pH dependent zeta potential for the silica particles

functionalized with mixed-monolayers of DMOAP and COOH-terminated silanes similar to COOH-terminated particles. The isoelectric point of particles was measured to be at pH = ~3.5. To control the adsorption of nanoparticles to droplet interfaces, we used suspensions at pH either 3 or 5.9 for these experiments. At pH = 3, the zeta potential of the droplets was measured to be -13.1 ± 2.4 mV, whereas that of nanoparticles were measured as +24.2 ± 15.5 mV. At pH = 5.9, the zeta potential of the droplets was -56.1 ± 7.0 mV and that of the particles was -33.1 ± 8.6 mV. Figure 4.20A shows the configuration distributions of the droplets that were incubated in 4 x 10^{10} particle/mL suspensions of particles at either pH = 3 or 5.9. In measurements at pH = 3, we observed 99.3 ± 0.9% of the droplets to maintain preradial configuration. However, for the measurements at pH = 5.9 resulted in only 3.9 ± 2.8% of the droplets to maintain preradial configurations, the rest of which was observed to be bipolar. Such configuration distribution of droplets at pH = 3, given that the particle concentration is high enough for surface coverage and the enhanced adsorption due to the opposite charges of the droplets and particles, indicates that the anchoring of 5CB on the surfaces of particles to be homeotropic (or tilted). Additional evidence on the homeotropic anchoring of 5CB on DMOAP/COOH mixed monolayer-coated particles are shown in Figure 4.20B, which presents the configuration statistics of the droplets as a function of nanoparticle concentration. As reported, the droplets were shown to maintain bipolar configuration at concentrations of ~ 4 x 10^{9} particles/mL, whereas the total frequency of preradial and radial configurations are dominant for higher particle concentrations. For adsorption at pH = 5.9, the charge repulsion of the particles and droplets resulted in the lower adsorption of the particles to the surfaces of the droplets, therefore resulted in bipolar configuration in the majority of the droplets.

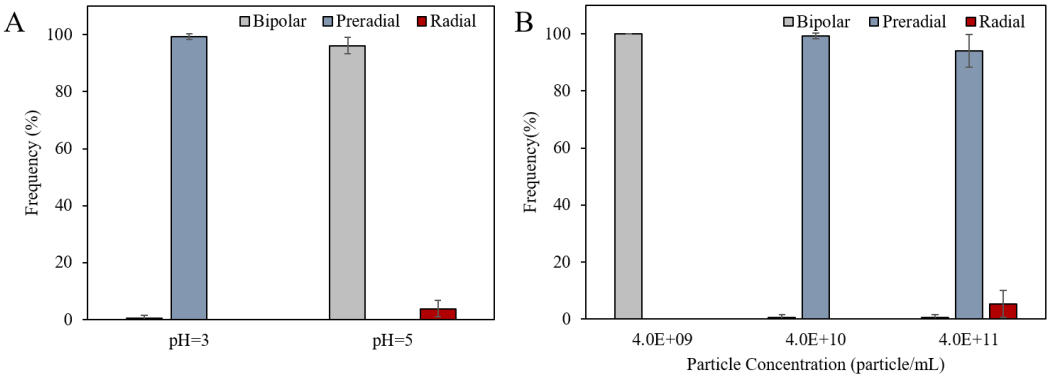

Figure 4.20 Configuration distribution of 5CB droplets dispersed in suspensions of silica particles coated with mixed monolayers of -COOH-terminated silanes and DMOAP. Average configurations of the droplets with respect to (A) pH of the suspension, (B) particle concentration.

Also, we quantified the temporal changes in the frequency of the droplet configurations incubated in suspensions. When the configuration statistics of the 5CB droplets present in suspensions of DMOAP/-COOH mixed monolayer-coated particles at pH = 5.9 were collected with respect to time, we observed the frequency of the droplet configurations with either preradial or radial to increase with time. As shown in Figure 4.21A, the total frequency of the droplets incubated in suspensions of DMOAP/-COOH mixed monolayer were measured to be 96.1 ± 2.8% bipolar after the measurements were collected at 10 min. However, the droplets to maintained 76.3 ± 10.7% bipolar at 60 min, and 12.8 ± 3.5% bipolar (79.9 ± 7.5% preradial and 7.3 ± 6.2% radial) at 90 min. The increase in the frequencies corresponding to radial and preradial configurations indicated an increased adsorption of particles to the surfaces of the droplets. The SEM microscopy studies shown in Figure 4.21D show that the density of the adsorbed nanoparticles was significantly increased with time for the experiment performed at pH=5.9, whereas the density of the droplets was high even after 10 mins when the experiment was performed at pH=3.

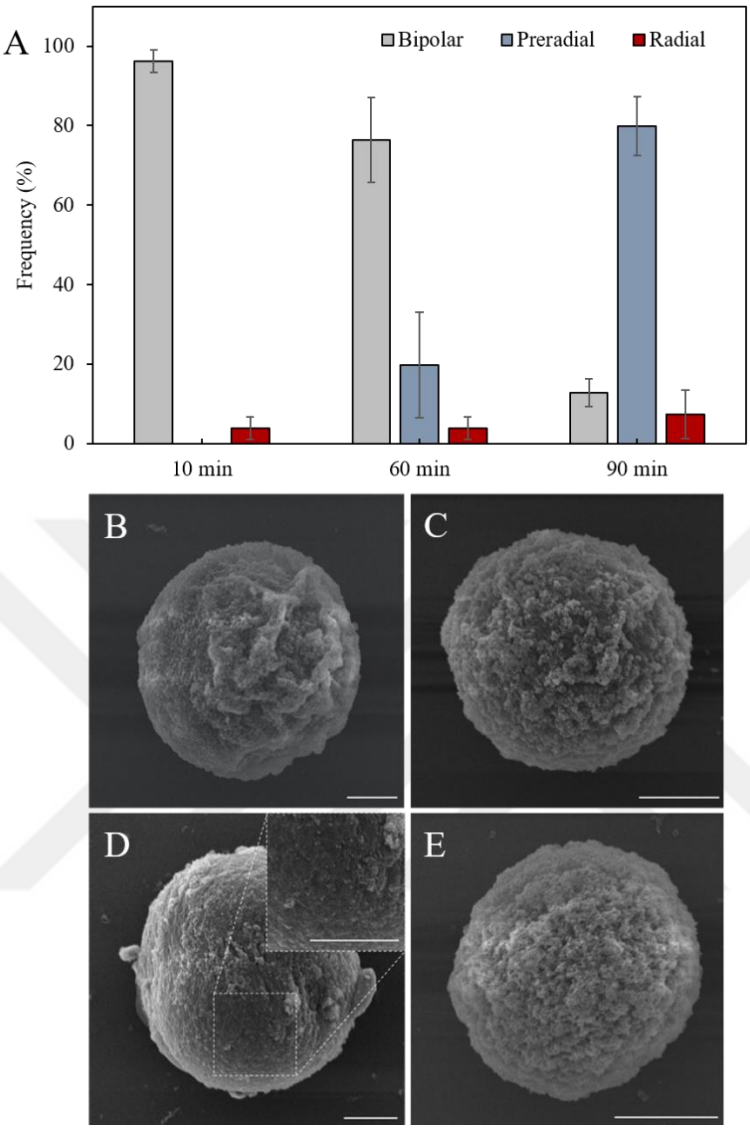

Figure 4.21 (A) Configuration distribution of 5CB droplets dispersed in suspensions of silica particles coated with mixed monolayers of -COOH-terminated silanes and DMOAP with respect to time. (B-D) Scanning electron micrographs of the polymerized LC droplets after contacting with suspensions of silica nanoparticles functionalized with mixed monolayers of -COOH-terminated silanes and DMOAP. Representative images of the droplets collected at (B, C) pH = 3 and (D, E) pH = 5. The images were collected from polymerized droplets of 25% wt RM257/5CB mixture after equilibration for (B,D) 10 mins, and (C,E) 90 mins in the suspensions. Inset in (D) shows the magnified image of the area indicated by dashed lines. Scale bars: 5 μm.

Herein, we also highlight the differences of the measurements collected from the droplets incubated in suspensions of DMOAP-coated nanoparticles compared to the

experiments performed with DMOAP/COOH mixed monolayer-coated particles. As shown in Figure 4.11A, the adsorption of the nanoparticles on 5CB droplets revealed configuration distributions with majority of the total number of the preradial and radial droplets shortly after the incubation of the droplets in the suspensions (~ 10 mins). However, we observed a time-dependent configuration distribution of the droplets when incubated in suspensions of DMOAP/COOH mixed monolayer-coated particles at pH = 5.9. We reasoned that this difference in the temporal changes droplet configuration statistics to result from the differences in the hydrophobicity and the charges of the particles. Thus, the results reported herein to highlight not only the surface anchoring of 5CB on particle surfaces but also the hydrophobicity or the charges of the particles relative to the droplet interfaces to provide access to the information regarding the physicochemical properties of the nanoparticles through the observations on the configuration statistics of the LC droplets.

In the last set of the experiments we performed, we investigated the effect of nanoparticle size on the response of LC droplets. For this purpose, we functionalized 50 nm silica nanoparticles with DMOAP and -COOH terminated silane groups. Then, we performed experiments using these nanoparticles and quantified the response of 5CB droplets upon the adsorption of the nanoparticles. First, we performed experiments with DMOAP-coated nanoparticles and examined the response of 5CB droplets upon adsorption of the nanoparticles. As we mentioned before, 5CB droplets maintained either radial or preradial configurations upon exposure to 100 nm-sized DMOAP-coated nanoparticles. In the experiments with smaller particles, 5CB droplets exhibited either preradial or radial configurations 84.9% of the total number for nanoparticle concentrations of 3.2×10^9 particles/mL as shown in Figure 4.22A. Also, with decreasing nanoparticle concentration, we observed a decrease in the total frequency of the preradial and radial configurations similar to 100 nm-sized silica nanoparticles.

Then, we examine the effect of nanoparticle size on LC droplet response with the adsorption of -COOH terminated nanoparticles to the LC-aqueous interface. 5CB droplets maintained 100% bipolar configuration upon the adsorption of -COOH

terminated particles with concentrations of 3.2 x 10^9 particles/mL as shown in Figure 4.22B. Since configuration distributions of LC droplets with 50nm silica nanoparticles are similar to our observations with 100 nm-silica nanoparticles which were given as 85.0 ± 6.9% bipolar configurations for -COOH terminated nanoparticles in Figure 4.17A and 90.1 ± 6.4% preradial or radial configurations for DMOAP-coated nanoparticles in Figure 4.12 before, we conclude that the response of 5CB droplets does not depend on the size of surface-functionalized nanoparticles.

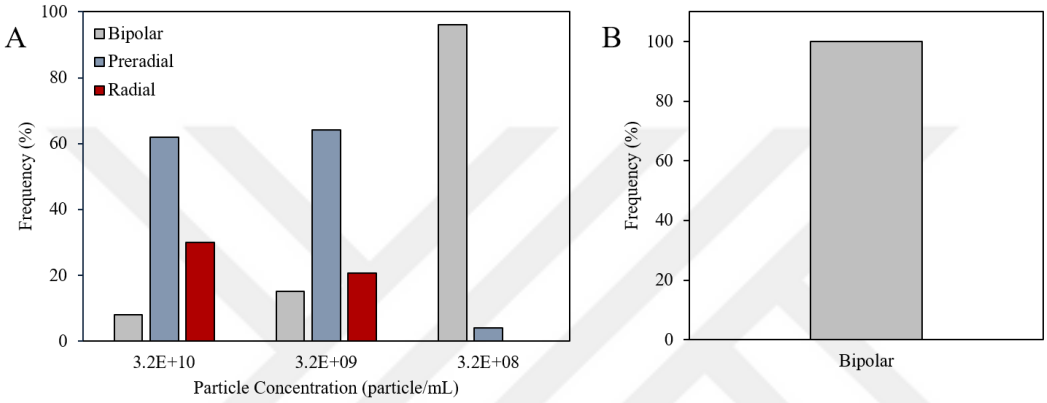

Figure 4.22 (A) Configuration distributions of 5CB droplets present in suspensions of different DMOAP-coated nanoparticle concentrations, (B) Configuration distributions of 5CB droplets present in suspensions of -COOH terminated silica nanoparticles

Overall, our results reveal that the physicochemical properties of surface-modified nanoparticles can be discovered through the temporal and equilibrium response of the LC droplets. This concept not only provides insight in nanoparticle detection but also gives information for the diagnosis of nano-sized species as viruses. Detection of such species provided through their surface properties regardless from their core structure. Surfaces of nanoparticles can be modified by mimicing the surface properties of viruses. Then, LC response upon the adsorption of nanoparticles can be examined to gain insight for the detection of this type of viruses. Moreover, our results show that LC droplets show a concentration-dependent response that can also be used in virus detection.

Alternatively, -COOH terminated silica nanoparticles can be used for the detection of biomolecules. Silica-based materials have been used extensively as a substrate material for biosensing and diagnostic applications.[51,52] For these applications, surfaces of the substrate must be modified with proper groups for the attachment of targeted biomolecules. -COOH terminated groups are commonly used in surface functionalization for effective immobilization of biomolecules such as aptamers, enzymes and antibodies.[53,54] Therefore, this study can be broadened for potential applications involving the immobilization of biomolecules and their detection using LCs.

As a further improvement of our study, an alternative characterization method can be used instead of microscopy since it is time consuming method when a population of droplets need to be characterized. Analysis methods such as flow cytometry can be used for characterization of the LC droplet configurations in an emulsion. Using this method, frequency of the director configurations of LC droplets can be determined with high precision based on different light scattering properties of these configurations.[55]

CHAPTER 5

CONCLUSION

We examined the response characteristics of nematic LC droplets upon the adsorption of surface functionalized nanoparticles at LC-aqueous interfaces. Our study differed from their past counterparts that investigated the droplet responses mostly against molecular species or micrometer-sized particles. We investigated the response of LC droplets present in concentrated nanoparticle suspensions and showed a concentration- and surface property-dependent configurations of the LC droplets upon adsorption of the nanoparticles to the LC-water interfaces. The equilibrium and the temporal response of the droplets provided information about the physicochemical properties of the nanoparticles such as charging, wetting and surface anchoring. Also, influence of nanoparticle size on the response of droplets was examined by using different surface groups. This study provides fundamental information and experimental methods that can form basis for future applications that employ nanoparticles at the interfaces of LCs. First, the findings we arrived herein can be used to develop sensors for the nanoscopic species, for example virus or bacteria. Second, the methods we followed in this study can be employed in the synthesis of composite microparticles with complex internal structuring. Third, the study can further be extrapolated to design sensors that employ nanoparticle-LC interactions. Although, the study itself opens new paths towards such important and critical applications, future studies can also be designed to (*i*) finely tune the interparticle interactions to investigate the self-assembly of the particles at the interfaces of confined elastic medium, (*ii*) to control the surface heterogeneity of the particles at the interfaces of LCs, (*iii*) to investigate the response of LC medium upon exposure to external stimuli that can interact with either the particles or the LC medium (such as light, magnetic field, electric field, etc.). Lastly, this study and the forthcoming studies may also benefit from the presence of more complex LC phases

confined in droplets, especially the cholesterics, smectics and blue phase liquid crystals.

REFERENCES

1. Bukusoglu, E., Pantoja, M. B., Mushenheim, P. C., Wang, X. & Abbott, N. L. Design of Responsive and Active (Soft) Materials Using Liquid Crystals. *Annu. Rev. Chem. Biomol. Eng.* **7**, 163–196 (2016).

2. Lin, I. H. *et al.* Endotoxin-induced structural transformations in liquid crystalline droplets. *Science.* **332**, 1297–1300 (2011).

3. Volovik, G. E. & Lavrentovich, O. D. Topological dynamics of defects: boojums in nematic drops. *Sov. Phys. JETP* **58**, 1159–1166 (1983).

4. Prischepa, O. O., Shabanov, A. V. & Zyryanov, V. Y. Transformation of director configuration upon changing boundary conditions in droplets of nematic liquid crystal. *JETP Lett.* **79**, 257–261 (2004).

5. Gupta, J. K., Zimmerman, J. S., De Pablo, J. J., Caruso, F. & Abbott, N. L. Characterization of adsorbate-induced ordering transitions of liquid crystals within monodisperse droplets. *Langmuir* **25**, 9016–9024 (2009).

6. Miller, D. S., Wang, X. & Abbott, N. L. Design of functional materials based on liquid crystalline droplets. *Chem. Mater.* **26**, 496–506 (2014).

7. Gupta, J. K., Sivakumar, S., Caruso, F. & Abbott, N. L. Size-dependent ordering of liquid crystals observed in polymeric capsules with micrometer and smaller diameters. *Angew. Chemie - Int. Ed.* **48**, 1652–1655 (2009).

8. Seo, J. M., Khan, W. & Park, S. Y. Protein detection using aqueous/LC interfaces decorated with a novel polyacrylic acid block liquid crystalline polymer. *Soft Matter* **8**, 198–203 (2012).

9. Aliño, V. J., Pang, J. & Yang, K. L. Liquid crystal droplets as a hosting and sensing platform for developing immunoassays. *Langmuir* **27**, 11784–11789 (2011).

10. Khan, W. & Park, S. Y. Configuration change of liquid crystal microdroplets coated with a novel polyacrylic acid block liquid crystalline polymer by protein adsorption. *Lab Chip* **12**, 4553–4559 (2012).

11. Brake, J. M., Daschner, M. K. & Abbott, N. L. Formation and characterization of phospholipid monolayers spontaneously assembled at interfaces between aqueous phases and thermotropic liquid crystals. *Langmuir* **21**, 2218–2228 (2005).

12. Brake, J. M., Daschner, M. K., Luk, Y. Y. & Abbott, N. L. Biomolecular Interactions at Phospholipid-Decorated Surfaces of Liquid Crystals. *Science.* **302**, 2094–2097 (2003).

13. Brake, J. M. & Abbott, N. L. An experimental system for imaging the reversible adsorption of amphiphiles at aqueous-liquid crystal interfaces. *Langmuir* **18**, 6101–6109 (2002).

14. Brake, J. M., Mezera, A. D. & Abbott, N. L. Effect of surfactant structure on the orientation of liquid crystals at aqueous-liquid crystal interfaces. *Langmuir* **19**, 6436–6442 (2003).

15. Brake, J. M., Mezera, A. D. & Abbott, N. L. Active Control of the Anchoring of 4′-Pentyl-4-cyanobiphenyl (5CB) at an Aqueous-Liquid Crystal Interface by Using a Redox-Active Ferrocenyl Surfactant. *Langmuir* **19**, 8629–8637 (2003).

16. Lockwood, N. A., De Pablo, J. J. & Abbott, N. L. Influence of surfactant tail branching and organization on the orientation of liquid crystals at aqueous-liquid crystal interfaces. *Langmuir* **21**, 6805–6814 (2005).

17. Sivakumar, S., Wark, K. L., Gupta, J. K., Abbott, N. L. & Caruso, F. Liquid crystal emulsions as the basis of biological sensors for the optical detection of bacteria and viruses. *Adv. Funct. Mater.* **19**, 2260–2265 (2009).

18. Koenig, G. M., Lin, I. H. & Abbott, N. L. Chemoresponsive assemblies of

microparticles at liquid crystalline interfaces. *Proc. Natl. Acad. Sci. U. S. A.* **107**, 3998-40031 (2010).

19. Lavrentovich, O. D. Transport of particles in liquid crystals. *Soft Matter* **10**, 1264–1283 (2014).

20. Khan, I., Saeed, K. & Khan, I. Nanoparticles: Properties, applications and toxicities. *Arab. J. Chem.* **12**, 908–931 (2019).

21. Wilczewska, A. Z., Niemirowicz, K., Markiewicz, K. H. & Car, H. Nanoparticles as drug delivery systems. *Pharmacol. Reports* **64**, 1020–1037 (2012).

22. Saha, K., Agasti, S. S., Kim, C., Li, X. & Rotello, V. M. Gold nanoparticles in chemical and biological sensing. *Chem. Rev.* **112**, 2739–2779 (2012).

23. Korzeniowska, B., Nooney, R., Wencel, D. & McDonagh, C. Silica nanoparticles for cell imaging and intracellular sensing. *Nanotechnology* **24**, 442002 (2013).

24. Esteves, C., Ramou, E., Porteira, A. R. P., Moura Barbosa, A. J. & Roque, A. C. A. Seeing the Unseen: The Role of Liquid Crystals in Gas-Sensing Technologies. *Adv. Opt. Mater.* **8**, (2020).

25. Malone, S. M. & Schwartz, D. K. Macroscopic liquid crystal response to isolated DNA helices. *Langmuir* **27**, 11767–11772 (2011).

26. Lockwood, N. A., Gupta, J. K. & Abbott, N. L. Self-assembly of amphiphiles, polymers and proteins at interfaces between thermotropic liquid crystals and aqueous phases. *Surf. Sci. Rep.* **63**, 255–293 (2008).

27. Mondiot, F., Wang, X., de Pablo, J. J. & Abbott, N. L. Liquid crystal-based emulsions for synthesis of spherical and non-spherical particles with chemical patches. *J. Am. Chem. Soc.* **135**, 9972–9975 (2013).

28. Rahimi, M. *et al.* Nanoparticle self-assembly at the interface of liquid crystal

droplets. *Proc. Natl. Acad. Sci. U. S. A.* **112**, 5297–5302 (2015).

29. Wang, X., Miller, D. S., De Pablo, J. J. & Abbott, N. L. Reversible switching of liquid crystalline order permits synthesis of homogeneous populations of dipolar patchy microparticles. *Adv. Funct. Mater.* **24**, 6219–6226 (2014).

30. Wang, X., Miller, D. S., de Pablo, J. J. & Abbott, N. L. Organized assemblies of colloids formed at the poles of micrometer-sized droplets of liquid crystal. *Soft Matter* **10**, 8821–8828 (2014).

31. Bukusoglu, E. *et al.* Positioning colloids at the surfaces of cholesteric liquid crystal droplets. *Soft Matter* **12**, 8781–8789 (2016).

32. Muševič, I., Škarabot, M., Tkalec, U., Ravnik, M. & Žumer, S. Two-dimensional nematic colloidal crystals self-assembled by topological defects. *Science.* **313**, 954–958 (2006).

33. Miller, D. S. & Abbott, N. L. Influence of droplet size, pH and ionic strength on endotoxin-triggered ordering transitions in liquid crystalline droplets. *Soft Matter* **9**, 374–382 (2013).

34. Moreno-Razo, J. A., Sambriski, E. J., Abbott, N. L., Hernández-Ortiz, J. P. & De Pablo, J. J. Liquid-crystal-mediated self-assembly at nanodroplet interfaces. *Nature* **485**, 86–89 (2012).

35. Sumer, Z. & Striolo, A. Nanoparticles shape-specific emergent behaviour on liquid crystal droplets. *Mol. Syst. Des. Eng.* **5**, 449–460 (2020).

36. Stöber, W., Fink, A. & Bohn, E. Controlled Growth of Monodisperse Silica Spheres in the Micron Size Range. *J. Colloid Interface Sci.* **26**, 62–69 (1968).

37. Manatunga, D. C., De Silva, R. M. & De Silva, K. M. N. Double layer approach to create durable superhydrophobicity on cotton fabric using nano silica and auxiliary non fluorinated materials. *Appl. Surf. Sci.* **360**, 777–788 (2016).

38. Koenig, G. M., De Pablo, J. J. & Abbott, N. L. Characterization of the reversible interaction of pairs of nanoparticles dispersed in nematic liquid crystals. *Langmuir* **25**, 13318–13321 (2009).

39. Shah, R. R. & Abbott, N. L. Using liquid crystals to image reactants and products of acid-base reactions on surfaces with micrometer resolution. *J. Am. Chem. Soc.* **121**, 11300–11310 (1999).

40. Schiestel, T., Brunner, H. & Tovar, G. E. M. Controlled surface functionalization of silica nanospheres by covalent conjugation reactions and preparation of high density streptavidin nanoparticles. *J. Nanosci. Nanotechnol.* **4**, 504–511 (2004).

41. Feifel, S. C. & Lisdat, F. Silica nanoparticles for the layer-by-layer assembly of fully electro-active cytochrome c multilayers. *J. Nanobiotechnology* **9**, 1–12 (2011).

42. Carlton, R. J., Gupta, J. K., Swift, C. L. & Abbott, N. L. Influence of simple electrolytes on the orientational ordering of thermotropic liquid crystals at aqueous interfaces. *Langmuir* **28**, 31–36 (2012).

43. Tjipto, E. *et al.* Tailoring the interfaces between nematic liquid crystal emulsions and aqueous phases via layer-by-layer assembly. *Nano Lett.* **6**, 2243–2248 (2006).

44. Wang, X., Bukusoglu, E. & Abbott, N. L. A practical guide to the preparation of liquid crystal-templated microparticles. *Chem. Mater.* **29**, 53–61 (2017).

45. Wang, X. *et al.* Synthesis of Optically Complex, Porous, and Anisometric Polymeric Microparticles by Templating from Liquid Crystalline Droplets. *Adv. Funct. Mater.* **26**, 7343–7351 (2016).

46. Rouet, P. E., Chomette, C., Adumeau, L., Duguet, E. & Ravaine, S. Colloidal chemistry with patchy silica nanoparticles. *Beilstein J. Nanotechnol.* **9**, 2989–2998 (2018).

47. Karem A. Court, Jackeline Jerez, R. J. R. and M. T.-L. Particle Encapsulation in Crosslinked Hydrogel Networks: Particle Distribution Optimization. *J. Mater. Sci. Eng. B* **10**, 539–550 (2012).

48. Karausta, A. & Bukusoglu, E. Liquid crystal-templated synthesis of mesoporous membranes with predetermined pore alignment. *ACS Appl. Mater. Interfaces* **10**, 33484–33492 (2018).

49. Akdeniz, B. & Bukusoglu, E. Design Parameters and Principles of Liquid-Crystal-Templated Synthesis of Polymeric Materials via Photolithography. *Langmuir* **35**, 13126–13134 (2019).

50. Akdeniz, B. & Bukusoglu, E. Liquid Crystal Templates Combined with Photolithography Enable Synthesis of Chiral Twisted Polymeric Microparticles. *Macromol. Rapid Commun.* **40**, 1900160 (2019).

51. Vashist, S. K., Lam, E., Hrapovic, S., Male, K. B. & Luong, J. H. T. Immobilization of antibodies and enzymes on 3-aminopropyltriethoxysilane-functionalized bioanalytical platforms for biosensors and diagnostics. *Chem. Rev.* **114**, 11083–11130 (2014).

52. Sonawane, M. D. & Nimse, S. B. Surface Modification Chemistries of Materials Used in Diagnostic Platforms with Biomolecules. *J. Chem.* **2016**, 19 (2016).

53. Bizid, S., Blili, S., Mlika, R., Haj Said, A. & Korri-Youssoufi, H. Direct Electrochemical DNA Sensor based on a new redox oligomer modified with ferrocene and carboxylic acid: Application to the detection of Mycobacterium tuberculosis mutant strain. *Anal. Chim. Acta* **994**, 10–18 (2017).

54. Cai, L., Chen, Z. Z., Dong, X. M., Tang, H. W. & Pang, D. W. Silica nanoparticles based label-free aptamer hybridization for ATP detection using hoechst33258 as the signal reporter. *Biosens. Bioelectron.* **29**, 46–52 (2011).

55. Miller, D. S., Wang, X., Buchen, J., Lavrentovich, O. D. & Abbott, N. L.

Analysis of the internal configurations of droplets of liquid crystal using flow cytometry. *Anal. Chem.* **85**, 10296–10303 (2013).